A Review of Aeronautical Fatigue Investigations in Sweden During the Period April 2023 to March 2025

Photo: Jörgen Ericsson, Copyright Saab AB

Edited by: **Zlatan Kapidzic**
Saab AB
Sweden

Saab Doc. No: LN-082174
Date: 19 March 2025

Presented at the 39th Conference of the International Committee on Aeronautical Fatigue and Structural Integrity (ICAF), Xi'an, China, 9-13 June 2025.

Table of Contents

1 INTRODUCTION

In this paper a review is given of the work carried out in Sweden in the area of aeronautical fatigue and structural integrity during the period April 2023 to March 2025. The review includes basic studies and industrial applications.

Contributions to the present review are from the following instances:

- Saab AB
  Sections 2.1, 2.2, 2.3, 2.4, 3.1, 4.1, 4.2, 4.3, 5.1, 6.1, 6.2, 6.3, 7.1

- Linköping University (LiU)
  Sections 3.1, 3.2

- Mid Sweden University (MiUn)
  Section 2.3, 2.4

- University West (UW)
  Sections 5.1

2 FATIGUE CRACK GROWTH AND LIFE PREDICTION METHODS

2.1 FE based method for calculation of fatigue life of lugs with arbitrary geometry and load direction

E. Lundqvist[1], *Z. Kapidzic*[1]

[1]Saab Aeronautics, Linköping, Sweden

Introduction

Lug joints are commonly used structural elements in aircraft design, whose function is to transfer force between two parts via the contact between a lug and a bolt. Lugs are generally subjected to cyclical loads, often with varying directions of force, which entails a risk of fatigue in the areas of high stresses. The existing fatigue sizing method for lugs is based on experimental data for a given reference lug geometry and correction factors based on the stress states and geometries of the reference lug and of the lug considered. Historically, the application of the sizing method has been limited to simple lug shapes and constant load directions, due to the difficulty to determine the stress history in a lug with arbitrary geometry and varying load direction.

In this study, we propose an update of the current method, based on a two-dimensional finite element (FE) stress solution of the contact problem in an arbitrary plane lug geometry. The work is currently on-going within a master's thesis project coordinated by Saab and Linköping University and is expected to be finalized by the beginning of June 2025. In this document we will present the fundamental ideas and the scope of the work, and the final results will be made available in the finalized version of the master's thesis.

Current fatigue sizing method

The principle of the currently used fatigue sizing method [1] is that the fatigue strength of an actual lug, defined by the nominal stress amplitude and mean stress (σ_a, σ_m) at N = const., is determined by scaling of the fatigue strength of a reference lug (σ_{0a}, σ_{0m}) with a factor ϕ_N. As the reference lug, a straight-sided, axially loaded lug with geometrical parameters a/c = 1, c/d = 1 and d = 10 mm is chosen, where d is the lug hole diameter while a and c are the axial and transverse ligament lengths. The correction factor is

$$\phi_N = 1 + \vartheta(k_1 k_2 - 1) \qquad (1)$$

where

$$k_1 = \left(\frac{a}{c}\right)^p \left(\frac{d}{c}\right)^q = \frac{K_{f0}}{K_f} \qquad (2)$$

is the shape factor, defined as the ratio of the fatigue notch factors of the reference lug and the actual lug and where

$$k_2 = \left(\frac{10}{d}\right)^n \qquad (3)$$

is the size factor, and where ϑ is a function of number of cycles to failure N.

As indicated in [1], the fatigue notch factors can be taken to be proportional to the stress concentration factors and the shape factor can therefore be calculated as the ratio of the latter. For straight-sided, axially loaded lugs the shape factor can thus written as function of a/c and d/c, using the closed-form solutions for the stress concentration factors of such lugs. For arbitrary lug geometries, such solutions are not available.

The idea in the current work is to develop an FE-program in Matlab, where a two-dimensional stress solution of the bolt-hole contact problem in an arbitrary plane lug geometry can be obtained. From the stress solution, the stress concentration factor is then calculated and used in Eq. (2) to determine the shape factor and subsequently the fatigue strength of the actual lug.

FE-model

The FE-approach utilizes the circumstance that lug geometries generally consist of a circular bolt hole and an outer perimeter which can easily be represented by spline curves defined by a number of points. Also, the load is always applied at the bolt and resisted at, usually, one of the perimeter segments. These circumstances offer a possibility to efficiently model arbitrary plane lug geometries and obtain on-the-fly solutions with simple inputs, thus eliminating the need for closed-form solutions.

Given the bolt-hole diameter and the points defining the outer perimeter of the lug, the program constructs a structured FE-mesh, for both the lug and the bolt, consisting of quadrilateral, plane stress or plane strain, elements. An example is shown in Fig. 2.1-1 (left), where the bolt elements are omitted. The stress solution is obtained for a force applied at the bolt center in a specified direction. Frictionless contact at the bolt-hole interface is enforced by formulation of Lagrange multiplicators directly at the conforming node pairs at the interface, and the solution is obtained generally in just a few iterations. Figure 2.1-1 (right) shows the deformed stress solution for an obliquely load example lug.

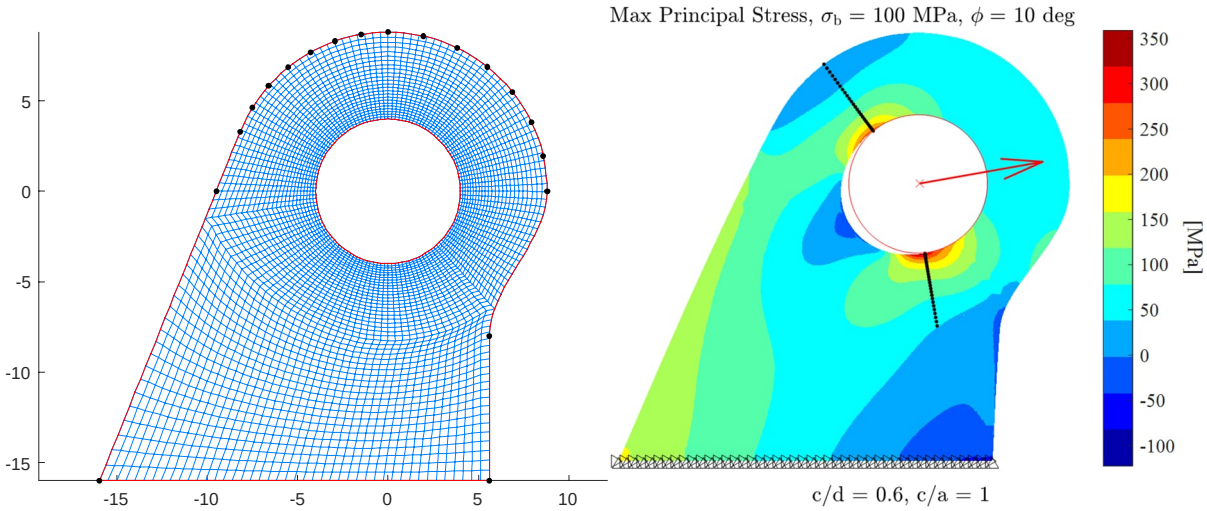

Figure 2.1-1. FE-mesh of an example lug (left) and the corresponding stress plot (right).

Generally two stress concentrations occur at the bolt-hole edge, where fatigue cracks can be expected to initiate. Therefore it is interesting to study the stress variation along the hole edge. Figure 2.1-2 shows plots of the contact pressure p, the bolt-hole gap g and the tangential stress σ_Θ normalized by the bearing stress σ_b and diameter, respectively, as function of the angle

coordinate Θ, for the lug shown in Fig. 2.1-1. Further we study the tangential stress distribution along radial lines emanating from the points of stress concentrations, see Figs. 2.1-1 and 2, in order to assess the stress concentration factor. Defining the nominal stress σ_n as the mean of the positive tangential stress along these lines we obtain the stress concentration factor as $K_t = \sigma_{\Theta max}/\sigma_n$.

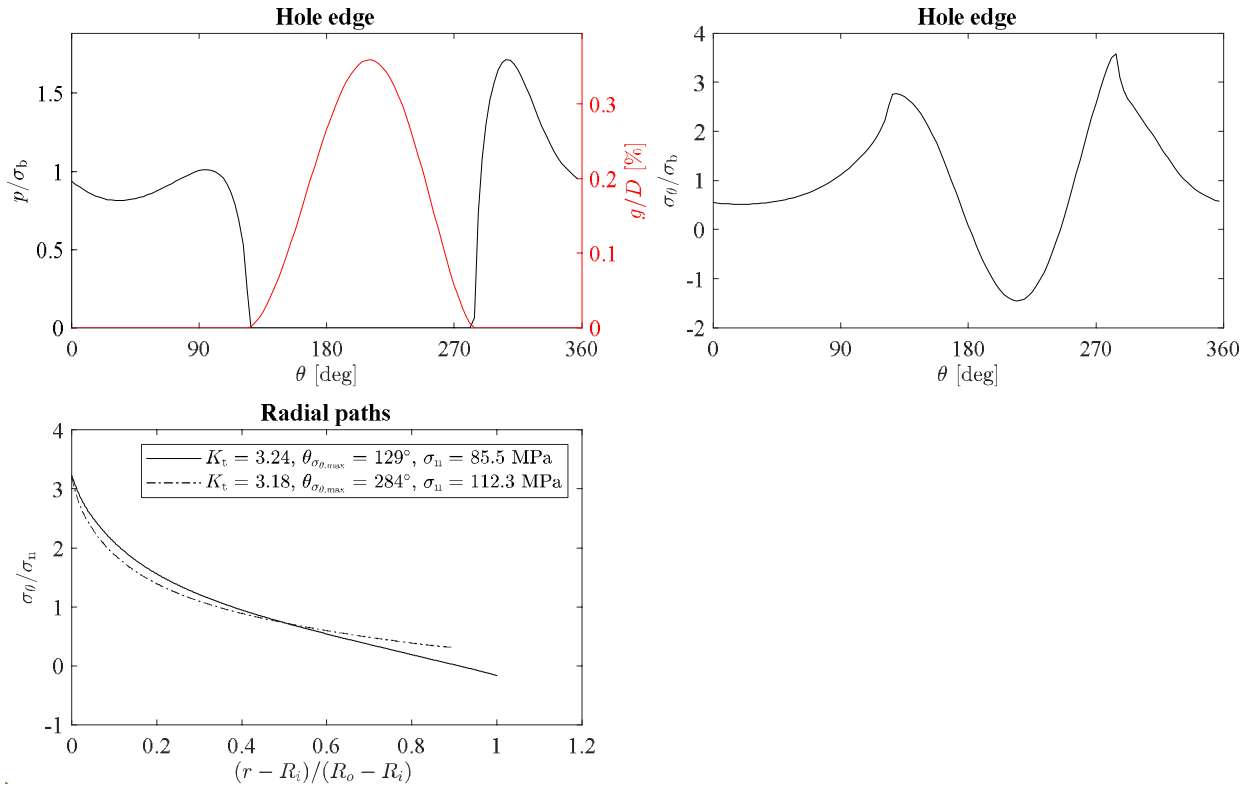

Figure 2.1-2. Normalized pressure, gap and tangential stress around the hole edge, and normalized tangential stress along radial paths.

Remaining and future work

So far we are able to determine the fatigue strength and fatigue life of a lug with an arbitrary outer geometry, loaded in a specified (constant) direction by using the FE-calculated K_t and σ_n in combination with Eqs. (1) - (3). Comparisons to test data on obliquely loaded lugs, which seems to be scarce in the literature, are currently being performed and are looking quite promising.

Calculating the cumulative damage sum for an arbitrary lug subjected to a variable amplitude load with a constant direction is straight forward using the method described above. However, accounting for a varying load direction and amplitude is slightly more challenging. For the most general case, we need to consider all points on the hole-edge as the potential fatigue crack initiation sites and determine the stress and the stress concentration histories associated with them. This is planned to be done, for a given time sequence of the force magnitude and direction, by superposition of the solutions of a series of scaled unit load cases involving different load directions which occur in the sequence and which can be solved using the proposed FE-model.

Other issues that are of interest for future studies and model development are: the effects of the contact friction, bolt-hole clearance, interference fitting, hole expansion and experimental validation of fatigue life in variable amplitude and direction loading.

References

[1] S. E Larsson. The development of a calculation method for the fatigue strength of lugs and a study of test results for lugs of aluminium. Proceedings of the 4th ICAF Symposium, 1969.

2.2 Fracture toughness testing of steel PH13-8Mo H1000/AMS 5934 (Extra High Toughness) using round bar specimens

Z. Kapidzic[1]

[1]Saab Aeronautics, Linköping, Sweden

Introduction

Stainless steel PH13-8Mo H1000/AMS 5934 (Extra High Toughness) is considered as an alternative to PH13-8Mo H1000/AMS 5629, due to its high fracture toughness properties. Typical applications are highly loaded critical parts which are designed for damage tolerance, e.g., large attachment or fitting bolts exposed to tensile or bending loads. In this context, the fracture toughness sizing values are of importance, particularly at low temperatures. Fatigue crack growth tests and fracture toughness tests are usually performed using CT-specimens, according to the ASTM standards in [1] and [2], to characterize the material fracture properties and to derive sizing data. Due to presumably high fracture toughness of AMS 5934, [2] requires a relatively large CT-specimen size in order to fulfill the plane strain condition in the fracture toughness test. This was deemed both costly and impractical due to the required specimen size and due to the restrictions of the available machine capacity.

In this study we performed fracture toughness test using round bar specimens of relatively smaller sizes instead. The motivation behind the choice of the specimen geometry, besides it being less costly and more practical, is that it is similar to the intended applications, i.e. bolts. The fracture toughness tests were performed in a tensile machine at different temperatures and the results were compared to corresponding values found in [3] and [4].

Test procedure

A number of specimens with threaded ends were manufactured, by machining from a 12 foot long round bar with diameter 1.5’’, see Fig. 2.2-1. A semi-circular initial defect of ~1.3 mm depth was introduced in the middle of each specimen by electro-spark machining.

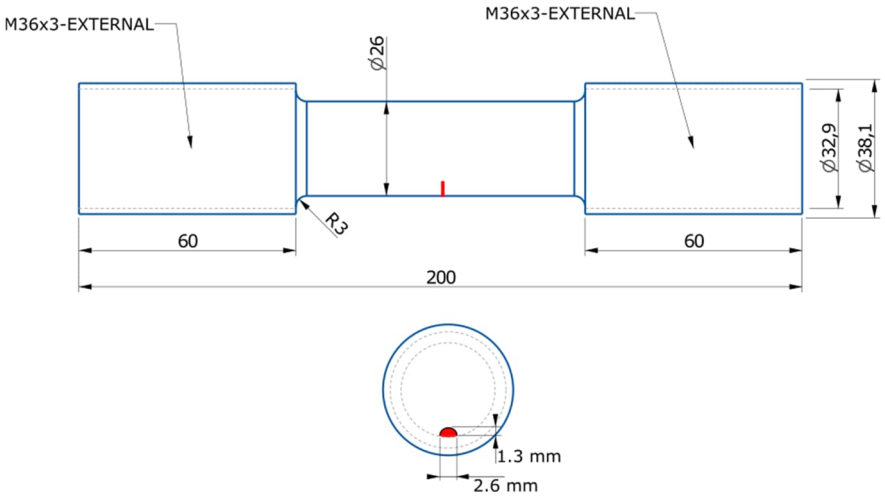

Figure 2.2-1. Specimen geometry and initial defect position.

Every specimen was first fatigued in a tensile machine at RT, at a load ratio R = -1 and with a relatively low applied force amplitude. During the cycling, the surface crack length $2c$ was monitored and measured using a usb-microscope. The specimen was fatigued until a predefined target surface crack length $2c_t$, was reached within reasonable accuracy. After the cycling, the surface crack length was also measured using eddy-current. The subsequent fracture tests were performed with these crack lengths, at different temperatures in the range of -50°C to RT.

The target surface crack lengths $2c_t$ were determined based on the anticipated fracture toughness values K_{IC} at different temperatures, obtained from [3] and [4], and a tradeoff between the calculated failure force and the net-section stress σ_n at failure, relative to the capacity of the tensile machine and the yield stress R_{p02}, respectively. Thus, for the tests at RT, larger $2c_t$ were calculated in order to reach the high K_{IC} at RT, using the upper force range of the tensile machine capacity. As a result of that, σ_n was also relatively large for the RT tests, although still lower than R_{p02}. For the tests at lower temperatures than RT, smaller $2c_t$ and σ_n were obtained.

Each specimen was tested to failure in a 1 MN machine. Prior to mounting into the machine, each specimen was equipped with a temperature sensor and placed in a climate chamber at an ambient temperature of about 10ºC less than the test target temperature for several hours. Thereafter, the specimen was removed from the climate chamber and tested to failure at ~500 kN/min, while the force, the machine grip displacement and the temperature were recorded.

Results

Two typical types of fracture mode were observed, denoted mode A and mode B, and shown in Figure 2.2-2. Residual failure in fracture mode A typically starts with a planar crack extension from a part of the in-depth crack front (denoted 1 in Fig. 2.2-2) and then changes to a ductile type of fracture with slanted fracture surfaces (denoted 2 in Fig. 2.2-2). Fracture mode B is planar across the whole cross-section of the specimen and is predominant at low temperatures, while mode A is predominant at RT.

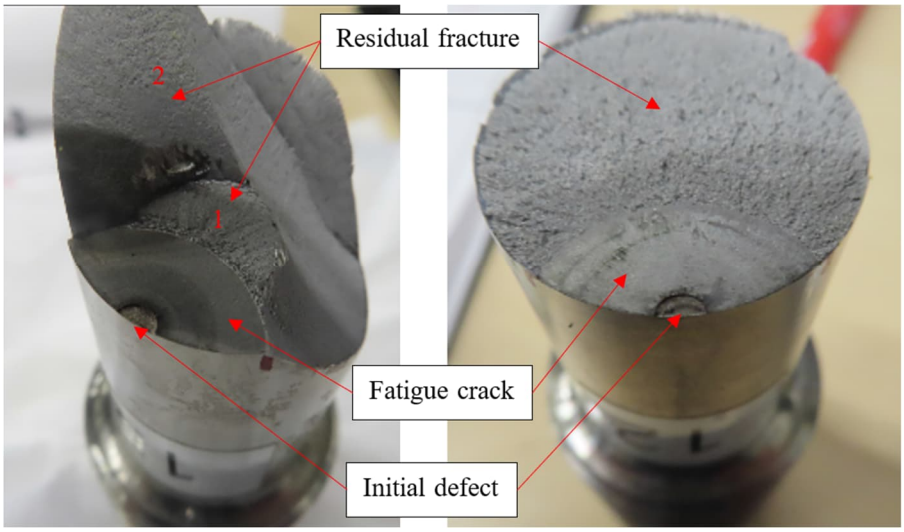

Figure 2.2-2. Fracture mode A (left) and B (right).

The conditional fracture toughness K_Q and the net-section stress σ_n were calculated based on: the *a posteriori* measured crack shape, the conditional failure force P_Q and the stress intensity factor solution for the in-depth crack point obtained from [5]. The crack shape was measured by fitting an ellipsis to the crack front in a microscope image of the fracture surface, see Fig.

2.2-3, and P_Q was determined based on a 95% secant (or a secant that corresponds to the stiffness reduction for a 2% crack extension) similar to the procedure in [2], see Fig. 2.2-4.

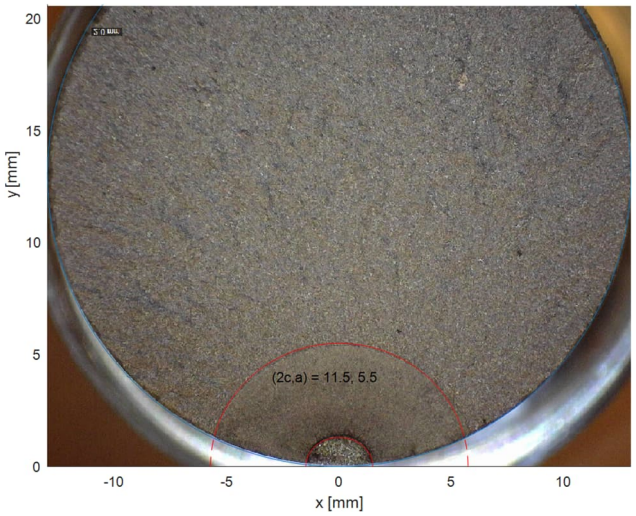

Figure 2.2-3. Measurement of crack shape.

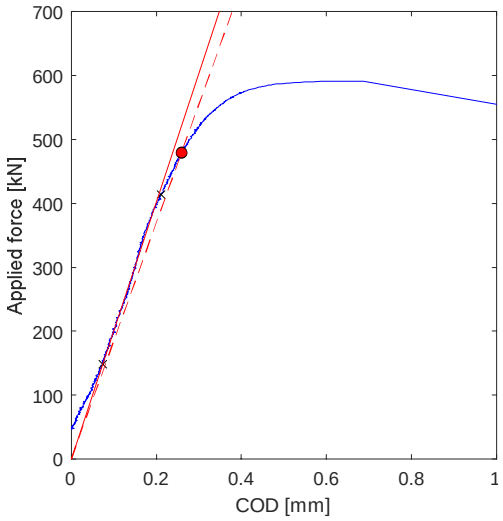

Figure 2.2-4. Determination of P_Q.

Although the net-section stress σ_n was < R_{p02} for all specimens, the ASTM [2] LEFM requirement regarding the ligament size, (D - a) < $2.5(K_Q/R_{p02})^2$, was only fulfilled for specimens that failed in mode B (filled markers in Fig. 2.2-5). Thus, following the reasoning in [2], the conditional fracture toughness values for the specimens tested at RT, which all failed in mode A, would be considered invalid. However, having the intended applications in mind, the ligament length (~0.62D) seen in the RT tests is a realistic scenario, both in sizing and structural testing situations. In such cases, the residual strength would normally be evaluated based on the criteria $K_I < K_{IC}$ and $\sigma_n < R_{p02,}$ regardless or the ASTM criterion. It is therefore plausible to consider the obtained RT values as useful for such situations, especially since the low-temperature values are sizing in most real situations anyways.

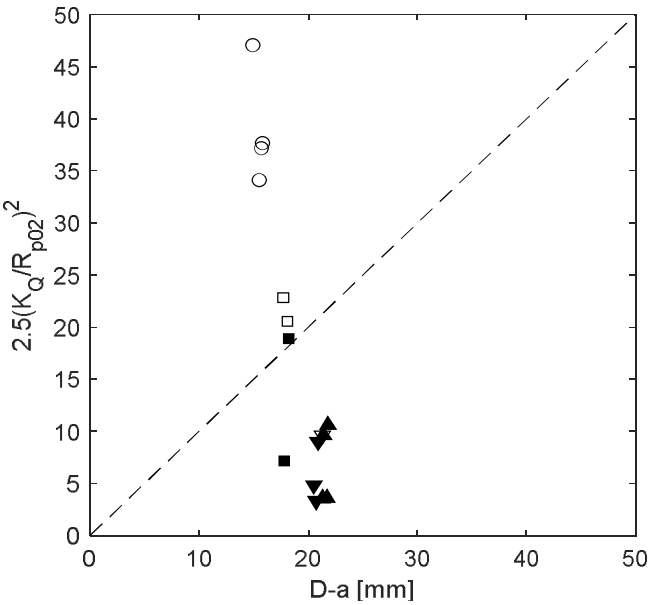

Figure 2.2-5. ASTM criterion related to the ligament, filled markers denote fracture mode B.

Following the argumentation above, we consider all obtained values and perform a linear regression analysis to determine the relation between K_Q and the temperature T, as well as to

compare with values from [3] and [4]. Figure 2.2-6 shows the mean regression line $K_Q(T)$ and the 95% confidence interval for the mean $E_{KQ}(T)$ together with the mean line from [4] and mean, max and min values at RT from [3], normalized with the mean from [3].

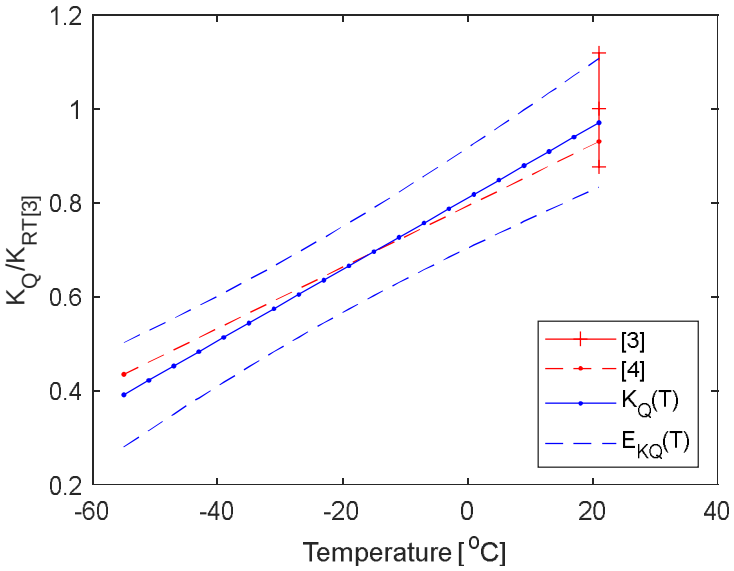

Figure 2.2-6. Fracture toughness normalized by RT value from [3], as function of temperature.

The obtained mean line correlates well with [3] at RT and with [4] over the entire temperature range. Conclusively, the demonstrated testing and analysis method resulted in fracture toughness values which are reasonably in line with known values, while significantly reducing the material and testing costs and simplifying the testing procedure.

References

[1] ASTM E647-15. Standard test method for measurement of fatigue crack growth rates.

[2] ASTM E399-22. Standard test method for linear-elastic plane-strain fracture toughness of metallic materials.

[3] MMPDS -10, Chapter 2 – Steel Alloys, FAA 2015.

[4] ATI Technical Data Sheet, 13-8 Supertough Alloy, Version 1, 2001.

[5] Shin C.S. and Cai C.Q. Experimental and finite element analyses on stress intensity factors of an elliptical surface crack in a circular shaft under tension and bending, International Journal of Fracture 129, 239-264, 2004.

2.3 Equivalent initial damage sizes for PBF-LB Ti-6Al-4V notched geometries

Z. Kapidzic[1], *S. B. Lindström*[2]

[1]Saab Aeronautics, Linköping, Sweden,
[2]Mid Sweden University, Sundsvall, Sweden

Introduction

For AM metal parts, the USAF Structures Bulletin [1] mandates the use of LEFM for durability and damage tolerance assessments and emphasizes the importance of defining a "surrogate damage" characterized by size, orientation, and location, based on the Equivalent Initial Damage Size (EIDS) distribution. EIDS is an analytical concept representing the initial quality of the structure and is derived from observed damage size distributions during testing or service.

In [2], Kapidzic et al. proposed a fracture mechanics-based method for determining the EIDS distribution in notched, as-built PBF-LB Ti-6Al-4V geometries. This article highlights some of the features of the proposed model and briefly discusses the obtained results.

Crack growth model

The model assumes a fatigue crack emanating from a semi-elliptical surface flaw located in the notch radius of an axially loaded round bar specimen. Given the initial depth of the flaw a_i, the aspect ratio of the flaw, an empirical crack growth rate law and the stress distribution over the specimen cross-section (stress concentration factor K_t), the model predicts the number of cycles to failure N_f, as function of the applied stress amplitude σ_a and load ratio R, thus

$$N_f = f(a_i, \sigma_a, K_t, R, \dots) \qquad (1)$$

Since the solution to Eq. (1) is obtained by an incremental scheme, the evolution of the fatigue crack shape is captured accounting for the effect of the varying stress field and the notch on the fatigue life. The effect of R is included directly through the crack growth rate law. Using the bisection method, Eq. (1) is solved for the initial flaw depth a_i obtaining

$$a_i = g(N_f, \sigma_a, K_t, R, \dots) \qquad (2)$$

for a given fatigue life N_f.

Results

In [2], an experimental program was conducted on specimens with different notch geometries tested at various load ratios. The experimentally obtained fatigue life N_f was then used with Eq. (2) to calculate the initial flaw depth a_i (EIDS) for each specimen corresponding to that fatigue life. The calculated set of the EIDS was then used to find a suitable distribution fit and for back-calculation of the SN-curves corresponding to percentiles of the EIDS distribution. Figure 2.3-1 shows a log-normal probability plot of a three-parameter Weibull-distribution fit to the data. It can be noted that the 99.9th percentile is 467.9 μm which exceeds the minimum required damage size of 254 μm for durability crack growth analysis stated [1].

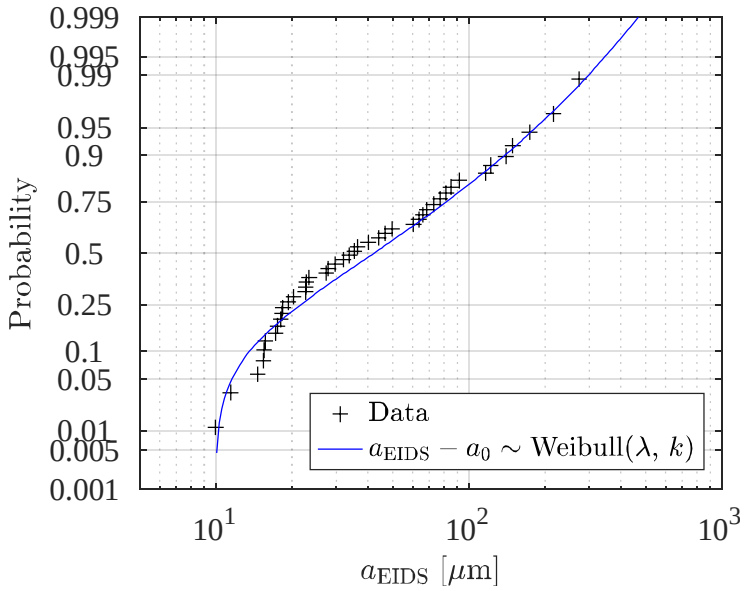

Figure 2.3-1. Log-normal probability plot of the EIDS distribution.

A *post mortem* microscope analysis of the fracture surfaces was performed on all specimens and it was concluded that the fatigue cracks initiated from the surface irregularities and defects but that they were difficult to characterize or quantify in terms of shape and size.

Prior to fatigue testing, the notch areas of the specimens were subjected to SEM surface roughness measurements. Comparisons were subsequently conducted to investigate if there is a relation between commonly used surface roughness parameters and the EIDS but no direct correlation was found. However, a correlation was found between the fatigue life obtained in the tests, N_f, and the predicted fatigue life, N_f (R_v), using the measured surface roughness parameter R_v as the initial flaw size, see Fig. 2.3-2. It was thus concluded that R_v is a fairly good estimate of EIDS.

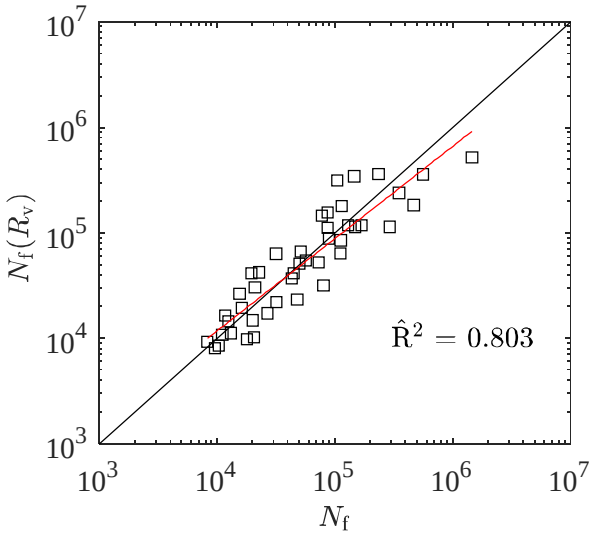

Figure 2.3-2. Fatigue life obtained by the tests, N_f, and the predicted fatigue life using measured surface roughness parameter N_f (R_v).

In conclusion, the proposed model offers a possibility of fatigue life predictions at different load ratios and extension to other notch geometries and load types, as well as informing variable

amplitude and non-proportional fatigue models, such as the one presented in section 2.4 of this document.

References

[1] Structures bulletin EZ-SB-19-01, durability and damage tolerance certification for additive manufacturing of aircraft structural metallic parts. Greene County, OH, USA: Wright Patterson Airforce Base; 2019.

[2] Z. Kapidžić, S. B. Lindström, J. Moverare, T. Lindström, C-J. Thore, D. Leidermark, M. Franke. Equivalent initial damage sizes for PBF-LB Ti-6Al-4V notched geometries, International Journal of Fatigue, 194, 108843, 2025.

2.4 Continuous-time, high-cycle fatigue modelling of AM titanium

S. B. Lindström[1], *Z. Kapidzic*[2], *T. Lindström*[2]

[1]Mid Sweden University, Sundsvall, Sweden,
[2]Saab Aeronautics, Linköping, Sweden

Introduction

Additive manufacturing (AM) is considered to have great potential for aerospace industry. Although the technique has been available for considerable time, most of the current applications are related to secondary, non-critical structures. One of the reasons for this is that the manufacturing process parameters greatly influence fatigue properties of AM produced parts. Nevertheless, efforts are currently being made to facilitate introduction of AM produced primary parts. Such parts can be expected to have complex geometries and to be exposed to complex loading with large magnitude. There is therefore a need to establish models that are capable of accurately predicting the fatigue life of AM components exposed to complex stress histories.

The continuous-time high-cycle fatigue model of Ottosen-Stenström-Ristinmaa (OSR) is relevant in this context. The model adapts to local conditions by accounting for stress-raiser effects through stress-gradient dependence and incorporating local surface roughness effects [1]. While originally developed for aluminum, it can be adapted to AM materials by considering the as-built surface defects and their dependence on the overhang. The OSR model is computationally efficient, introducing a relatively small overhead to calculations. Furthermore, it integrates easily into finite element modeling (FEM) and, due to its automated consideration of notch effects, fits smoothly into the design process.

A recent publication [2], presents an incremental fatigue damage model, based on work in [3], applied to fatigue of AM titanium.

Fatigue model

The OSR model uses the stress history $\boldsymbol{\sigma}(t)$ at a material point as input. Inspired by kinematic hardening models in plasticity, it is based on a moving endurance surface $\beta(\bar{\sigma}, I_1) = 0$ defined by an endurance function $\beta(\bar{\sigma}, I_1)$, with $I_1 = tr(\sigma)$ and $\bar{\sigma} = \sqrt{3/2}\,\|\boldsymbol{s} - \boldsymbol{\alpha}\|$. Here, $\|\boldsymbol{X}\|$denotes the Frobenius norm of a tensor $\boldsymbol{X}$, $\boldsymbol{s}$ is the deviatoric stress and $\boldsymbol{\alpha}$ is a backstress. The backstress and damage D are governed by an initial value problem

$$\dot{\boldsymbol{\alpha}} = (\boldsymbol{s} - \boldsymbol{\alpha})CH(\beta)H(\dot{\beta})\dot{\beta}, \qquad \boldsymbol{\alpha}(0) = \boldsymbol{0}, \tag{1}$$

$$\dot{D} = Kexp(L\beta)H(\beta)H(\dot{\beta})\dot{\beta}, \qquad D(0) = 0, \tag{2}$$

where H is Heaviside's step function and C, K, and L are positive model parameters. Size effects are captured by letting the endurance function parameters depend in the relative stress gradient [4].

Results

The OSR model was fitted to fatigue data for PBF-LB Ti6Al4V with as-built surfaces. Axisymmetric specimens were used, including smooth specimens and specimens with V-shaped circumferential notches with stress concentration factors of 2.2 and 3.0. Constant-amplitude (CA) loading was applied with different load ratios. The model was trained on these tests and additional fatigue data from the literature. Consequently, the scatter in the fit originated from both experimental variability and batch-to-batch differences. The observed scatter was slightly larger than previously reported for AA7075-T6 and AA7050-T7. Nevertheless, the results indicated that PBF-LB Ti6Al4V with as-built surfaces could be a viable material for primary structures in terms of reliability.

After training the OSR model using CA fatigue tests, out-of-phase CA tension-torsion experiments were conducted on circumferentially notched PBF-LB Ti6Al4V with as-built surfaces. The results showed that the OSR model's predictions for nonproportional multiaxial loading were within the experimental scatter or conservative. The conservativeness was particularly pronounced in oscillatory torsion without superimposed tension. In this case, the specimens exhibited factory rooftop fracture surfaces, which extended fatigue life due to friction along the tilted fracture planes.

There is nothing in the results that excludes the use of PBF-LB Ti6Al4V with as-built surfaces as a material for primary structures of aircraft. Although the S-N curves of PBF-LB Ti6Al4V with as-built surfaces fall at a lower stress level than those of machined PBF-LB Ti6Al4V, the scatter is lower. This is likely because machining does not remove all defects, thereby improving average fatigue resistance but not eliminating severe surface flaws. PBF-LB Ti6Al4V with as-built surfaces remains a viable option, as it preserves most of the design freedom associated with AM.

References

[1] S. B. Lindström, J. Moverare, J. Xu, D. Leidermark, R. Eriksson, H. Ansell, and Z. Kapidžić. Service-life assessment of aircraft integral structures based on incremental fatigue damage modeling, Int. J. Fatigue, 172:107600, 2023.

[2] S. B. Lindström, J. Moverare, M. Franke, J. Persson, D. Leidermark, C-J. Thore, T. Lindström, Z. Kapidžić. Fatigue life prediction for PBF-LB Ti6A14V with as-built surface under nonproportional loads using an incremental fatigue damage model, Int. J. Fatigue, 193, 108777, 2025.

[3] N. S. Ottosen, R. Stenström, and M. Ristinmaa. Continuum approach to high-cycle fatigue modeling, Int. J. Fatigue, 30(6):996–1006, 2008.

[4] Ottosen, N.S., Ristinmaa, M., Kouhia, R., Enhanced multiaxial fatigue criterion that considers stress gradient effects, Int. J. Fatigue, 116:128-139, 2018.

3 STRUCTURAL INTEGRITY OF COMPOSITESTRUCTURES

3.1 Experiments and modelling of composite-aluminium bolted joints

H. Wemming[1]

[1]Saab Aeronautics, Linköping, Sweden,
[2]Division of Solid Mechanics, Linköping University, Linköping, Sweden

Introduction

This chapter summarizes the continued work building on the research presented in the licentiate thesis [1], focusing on the structural integrity of composite-aluminium bolted joints. These joints are critical in aerospace applications, where bolted joint behaviour significantly affect the overall load-bearing capability of an assembly. Accurate modelling is essential for predicting joint performance and improving structural design.
Research is ongoing in two areas. The first is a development of the work in [2] and focuses on deriving Iwan model parameters for bolted joints using finite element (FE) simulations, developing a meta-model to predict fastener behaviour across different bolted joint geometries. The second examines the mechanical response of carbon fibre laminates in a half-hole pin bearing (HHB) test, emphasizing the effects of pin-hole friction on load transfer and laminate failure.

Parameter identification for fasteners in composite–aluminium bolted structures using simulation data

In [2], the deformation of composite-aluminium bolted joints under uniaxial quasistatic tension load is modelled using an Iwan model for each fastener. Experimental force-displacement data are used to determine the Iwan model parameters. In the present work, finite element (FE) simulations are used instead to identify suitable Iwan model parameters to represent the bolts in single-shear bolted lap joints.
FE models are developed for a handful of experimental specimens with varying geometries, using solid elements, contact, friction and nonlinear material response. The carbon fibre plate is modelled with an orthotropic elastic response expressed in terms of the Tsai's Modulus $\mathcal{T}$ [3], which requires only one parameter to describe the material stiffness, and an ideal plastic material model for inelastic behaviour. The stiffness $\mathcal{T}$ and yield limit are optimised to calibrate the FE models against experimental data.
Once the model parameters are calibrated, a large set of new FE models is generated with the same material and contact properties but different geometries. Iwan parameters are extracted from the simulated force-displacement curves. Finally, the simulated data are used to develop a meta-model that predicts Iwan parameters for various bolted joint geometries. The proposed model provides a computationally efficient structural element for analysing structures with multiple fasteners.

Compressive strength of half-hole pin bearing laminated carbon fibre specimens

This study investigates the mechanical response of laminated carbon fibre specimens under quasi-static compression loading using a half-hole pin bearing (HHB) test setup, see Fig. 3.1-

1. The HHB specimen is used to study pin-hole contact conditions and bearing damage in carbon fibre material under simpler local load conditions than standard bearing or full bolted joint tests.
The half-hole pin bearing specimens are manufactured from conventional open-hole specimens, cut in half to form a quasi-isotropic rectangular plate with a half hole on one edge. The specimens are compressed, forcing the hole edge against a steel pin matching the hole diameter. Force was measured using a calibrated load cell. Displacement was measured both from the machine grip displacement, and from an extensometer capturing the relative displacement between the specimen edge and the pin fixture.
Some specimens were analysed using digital image correlation (DIC), with a speckle pattern applied via spray-can paint. A significant experimental finding was a ~20% reduction in peak compressive load for DIC-painted specimens compared to unpainted ones. This effect, consistently observed for specimens with both 6 mm and 8 mm holes, is likely due to higher bearing friction force in unpainted specimens, which counteracts out-of-plane laminate expansion and increases the laminate's strength.
Finite element (FE) simulations complemented the experimental work, using a three-dimensional solid model with contact, friction and an orthotropic elastic response with ideal plastic inelastic behaviour. The FE model was calibrated against experimental data by optimizing stiffness and yield limit, while friction coefficients were varied to assess their effect on load transfer and failure mechanisms.
The findings underscore the importance of surface contact conditions in bolted joints. Understanding friction effects is essential for both experimental testing and numerical modelling of pin-hole contact, as these factors significantly influence mechanical performance. The HHB specimen geometry provides an efficient means of experimentally evaluating these effects.

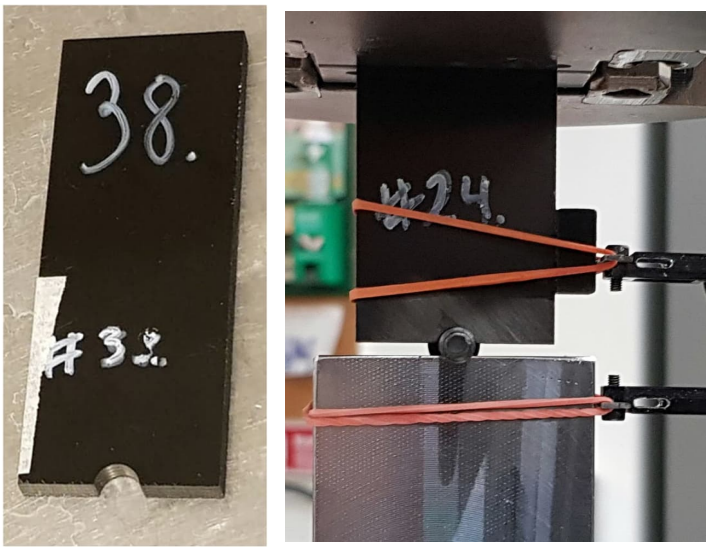

Figure 3.1-1. HHB specimen (left) and experimental setup (right) showing HHB specimen, steel pin and extensometer.

References

[1] H. Wemming. Experiments and modelling of composite–aluminium bolted joints. Linköping University Electronic Press, 2022. (Linköping Studies in Science and Technology. Licentiate Thesis.)

[2] H. Wemming, S. B. Lindström, L. Johansson, Z. Kapidžić. Modelling and experimental parameter identification for fasteners in composite–aluminium bolted structures, Composite Structures 323 (2023) 117464.
[3] S. W. Tsai, J. D. D. Melo, An invariant-based theory of composites, Composites Science and Technology 100 (2014) 237–243.

3.2 Mechanical performance of thin-ply composites for cryogenic applications

M. Loukil[1]

[1]Linköping University, Linköping, Sweden

Introduction

Aeronautical and aerospace applications are increasingly using composite materials such as carbon fiber/epoxy laminates, justified by their outstanding combination of properties, including high stiffness, strength, and low density. Despite these advantages, a significant challenge faced by composites in various applications is the occurrence and accumulation of micro-damage during their service life. When subject to increasing tension, a multi-layered composite laminate will eventually experience macroscopic failure. However, the ultimate failure is typically the result of multiple micro-damage mechanisms that initiate and develop throughout the loading history. In polymeric composites, the first mode of micro-damage often involves the formation of transverse (intralaminar) cracks in the off-axis layers. This is followed by the growth of delamination and the development of fiber breaks in adjacent plies around the tips of the transverse cracks, attributed to stress concentrations. The final macroscopic failure of the laminate depends on the sequence and extent of the micro-damage events during the loading history. Numerous studies have been published examining the effect of damage development in composite laminates on thermo-elastic properties [1-2]. Hence, to improve failure resistance and enhance the overall mechanical efficiency, it is desirable to inhibit the formation of micro-damage, especially the onset and progression of transverse cracks, which frequently act as the starting point for subsequent damage mechanisms.

An effective approach to suppress the formation of transverse cracks involves decreasing the thickness of the plies in the laminate. This reduction lowers the potential energy release rate (ERR) for crack propagation along the fiber direction within the ply, thereby demanding a greater applied load to initiate a tunneling crack [3-4].

Lower probability of significant defects in a thin layer can enhance resistance to cracking. Matrix cracking, delamination, and splitting damage occurring under static, fatigue, and impact loadings can be effectively postponed without the necessity for specialized resins or through-the-thickness reinforcements. Numerous experimental studies have substantiated this claim [5-6]. The impact of ply thickness on crack propagation mechanisms was examined in [5], where the energy release rate of intralaminar transverse cracks was investigated through finite element analysis. The investigation verified the crack suppression effect in thin-ply laminates, ultimately attributing this effect to a reduction in the energy release rate at the crack tip in the thin layer [5].

In this work, the effect of thermo-mechanical cycling of thin ply composites intended for cryogenic hydrogen storage applications was investigated. Mechanical quasi-static and fatigue as well as thermal fatigue tests were performed. Only a few matrix cracks were observed at very high load and high number of cycles. Those cracks were initiated but not propagated along the width of the specimens. These results show that thin ply composites have the potential to become viable material solutions for future lightweight hydrogen tanks.

Materials and manufacturing Use of this Template

The material in this study consisted of a dry TeXtreme® thin ply unidirectional UD band carbon reinforcement manufactured by Oxeon, which during the winding operation was impregnated by a special epoxy resin suited for cryogenic use. The thin ply UD bands were 20 mm wide, about 0.05 mm thick. Nominally [90/0]4s laminates were manufactured by filament winding of the impregnated bands on a flat 500 mm x 500 mm x 50 mm aluminium tool plate with 25 mm edge radius. The biaxial layup was realized by adjusting the holders at two diagonal corners of the tool plate. The winding was followed by a cure cycle of 24 h in +66°C and 4 h in +93°C.

Experimental results: Damage evolution in cross-ply laminates due to quasi-static tests

Damage evolution in cross-ply specimens subjected to tensile load was studied at room temperature.

Specimens were loaded and unloaded in steps. In each step a certain selected maximum strain level was reached after which the specimen was unloaded and taken out from the testing machine grips. After each loading step the polished edges of each specimen were studied under an optical microscope and the number of cracks was counted within the gage length of 50 mm in the middle of the specimen. Thereafter, the specimens were mounted back in the testing machine and subjected to the next loading step with a higher maximum strain level (by 0.2% higher than is the previous step). The manual counting of transverse cracks was performed after each load step.

The first investigations were done when no loading was applied during the inspection, however, transverse cracks were not clearly visible. Only fiber breaks were observed at very high applied strain and starting from 1.1% strain as it is shown in Fig. 3.2-1.

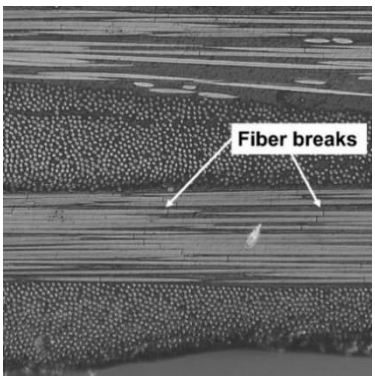

Figure 3.2-1. Fiber breaks at 1.5% strain.

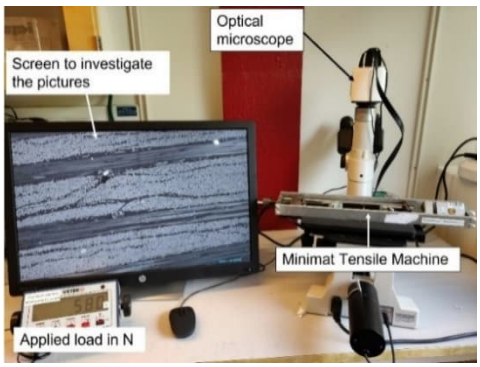

Figure 3.2-2. Specimen loaded during microscopic investigations.

For that reason, we have investigated the following options to open the matrix cracks if they existed:

Option 1: A small tensile machine (Minimat Tensile Testing Machine) was used while looking in the microscope. The maximum load applied with the small tensile machine was about 500 N which gives an equivalent strain of 0.04% which is considered as very low strain. Only fiber breaks were observed with this method. Figure 3.2-2 described how the small tensile machine looks and how it was used.

Option 2: The specimen's edge was coated with white paint while subjected to a load of 900 N (0.07% strain). The process involved applying white paint to the polished edge, allowing it to

penetrate the transverse cracks, removing the excess paint, and subsequently examining the edge using an optical microscope. By employing this approach, only two matrix cracks were detected following the specimen's loading up to 1.5%.

Option 3: Edge replication. A replica was used to identify cracks while the specimen was loaded to 0.1% of strain. This method involves the microscopic examination of surface replicas prepared by pressing a polymer against the specimen edge. Few cracks were observed using this method. Figure 3.2-3 presents a selection of matrix cracks captured at 1.6% applied strain.

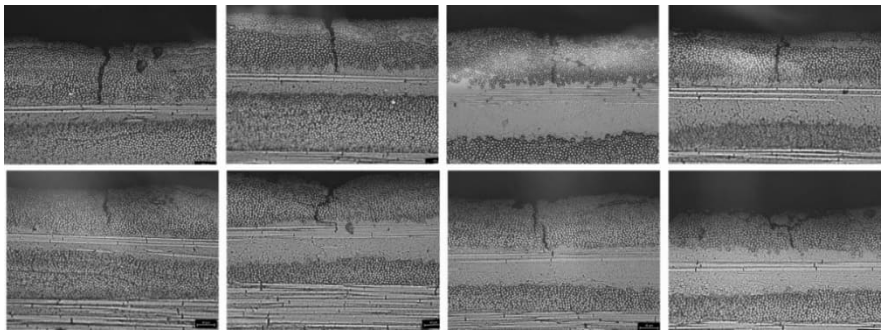

Figure 3.2-3. Transverse cracks observed in the surface 90 layer at 1.6% strain (0.1% was applied to open the cracks). Pictures taken from replica.

The evolving transverse crack initiation in the damaged 90-ply observed at the specimen edge is characterized by the “crack density”. The transverse crack density is calculated as the number of initiated transverse cracks per gage length Lg=50mm. Four specimens were tested. For specimen 1, only option 1 was used, and no transverse cracks were observed until failure. For specimen 2, option 1 and option 2 were employed resulting in the identification of a few transverse cracks. For specimen 3 and 4, option 3 was applied which led to the observation of a greater number of cracks. For all investigated specimens, only cracks on the surface 90 layers were observed. Significantly, fiber breakages became apparent in all specimens at an applied strain of 1.1%. Ultimately, specimen failure occurred within the range of 1.6% to 1.7% of the applied strain. The crack density as a function of applied for is shown in Figure 4. Transverse cracks were identified using option 3, and specimen 4 was thermally shocked 20 cycles (20 seconds at liquid nitrogen, and 10 min at 70 degree) before it was tested mechanically. The intension of using thermal shock was to investigate if the transverse cracks will appear faster than the unshocked specimen.

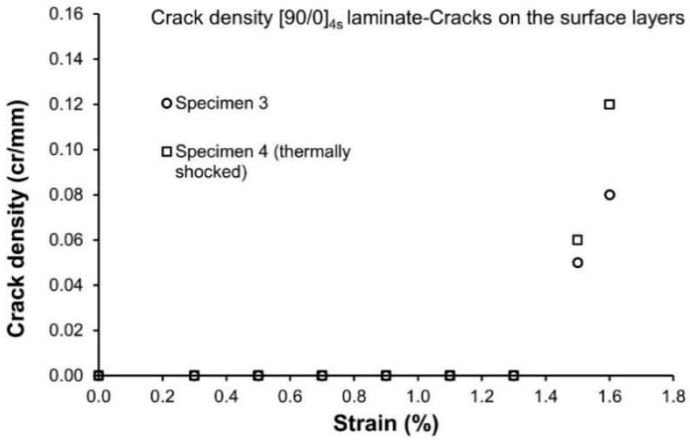

Figure 3.2-4. Crack density as a function of strain (cracks measured with replica).

Conclusions

Cross ply $[90/0]_{4s}$ composite laminates were manufactured using filament winding. The laminates were inspected, and specimens prepared for testing. Quasi-static tests were performed. Only a few matrix cracks were observed at very high load. Those cracks were initiated but not propagated along the width of the specimens. The test results showed that the material has a high damage onset level and therefore makes it an interesting candidate to make hydrogen composite tanks and pipes. The limited damage indicates that there are no obvious leak paths through the thickness that would compromise the functionality of the material in this application.

References

[1] Varna J, Loukil MS, Pupurs A, Joffe R. Damage and Failure Analysis for Composites Comprehensive Structural Integrity, 2023; V3-225 - V3-246.

[2] Loukil MS, Varna J, Ayadi Z. Engineering expressions for thermo-elastic constants of laminates with high density of transverse cracks, Composite Part A: Applied Science and Manufacturing 2013; 48(1):37-46.

[3] Parvizi, A., Garrett, K.W., Bailey, J.E. Constrained cracking in glass fibre-reinforced epoxy cross-ply laminates (1978) J Mater Sci, 13 (1), 195-201.

[4] Dvorak, G.J., Laws, N. Analysis of first ply failure in composite laminates (1986) Eng Fract Mech, 25 (5-6), 763-770.

[5] Saito, H., Takeuchi, H., Kimpara, I. Experimental evaluation of the damage growth restraining in 90° layer of thin-ply CFRP cross-ply laminates (2012) Adv Compos Mater, 21 (1), 57-66.

[6] Amacher, R., Cugnoni, J., Botsis, J., Sorensen, L., Smith, W., Dransfeld, C. Thin ply composites: Experimental characterization and modeling of size-effects (2014) Compos Sci Tech, 101,121-132.

4 FULL-SCALE FATIGUE TESTING

4.1 Damage tolerance test verification programme for Gripen E/F airframe

Z. Kapidzic[1], *P. Haugskott*[1]

[1]Saab Aeronautics, Linköping, Sweden

Service life and damage tolerance capability of the airframe structure need to be verified by testing. The tests can either be based on similarities to previously conducted tests, if applicable, or by new tests when no previous test results are available. Full-scale testing is required when:

- Changed design principles in primary load paths
- Changed material in safety-of-flight critical parts
- Significant change of stress conditions in legacy primary load paths

When Gripen A/B was initially developed, the test verification task was huge since all of the above criteria applied. Especially the implementation of the damage tolerance task according to the MIL-A-83444 specification called for test verification. An extensive fatigue and damage tolerance test program of full-scale test assemblies was accomplished, see Fig. 4.1-1. Both airframe and systems parts, e.g. actuators in the flight control system, were included and a total of about 800 artificial defects, sizing between .05 and .25 inch, were introduced in the structural parts and in the correct structural surroundings. In addition conventional full-scale static and fatigue tests of both A and B versions were conducted covering testing beyond ultimate loads and 4 lifetimes respectively.

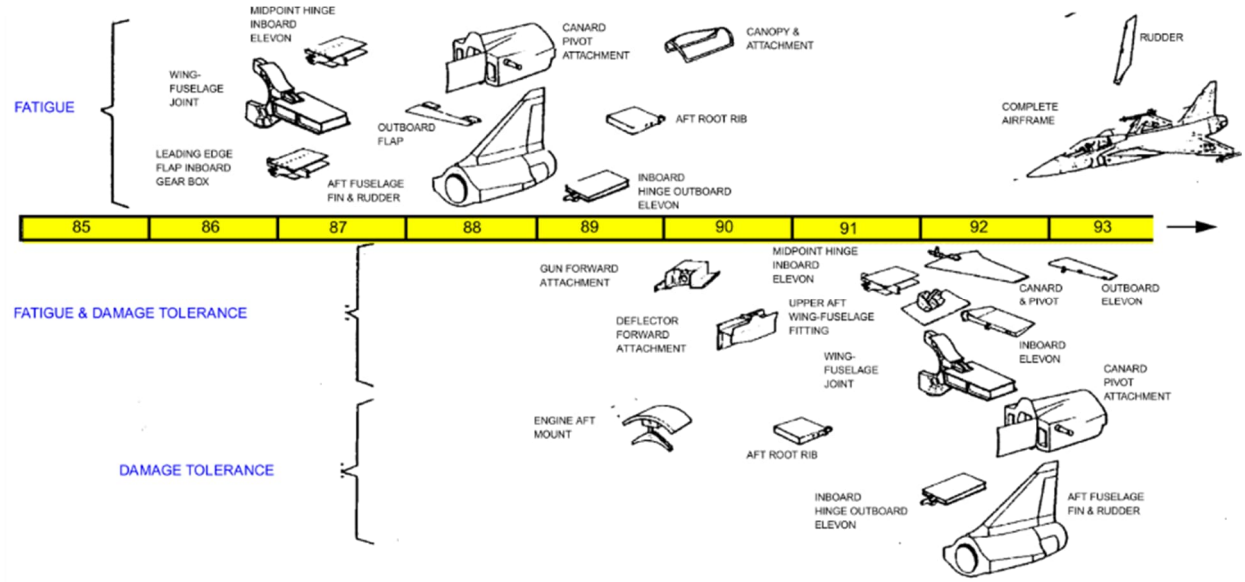

Figure 4.1-1. Test programme for fatigue and damage tolerance verification of Gripen A/B airframe.

When Gripen C/D was developed, no change of materials was done and no change of major load paths. Essential changes of local geometries were however done through the redesign to integral structures, extended service life (from 4,000 to 8,000 hours) and increased basic design mass (~10% compared to A/B versions) and some other load and structural changes, e.g. air-to-air refueling probe, called for new full-scale fatigue tests, se Fig. 4.1-2. Damage tolerance tests were however not done in any large extent since the load path were the same although

redesigned but the validation effort done on the fracture mechanic based damage tolerance methods during the A/B developments were deemed to be sufficient also for the C/D versions.

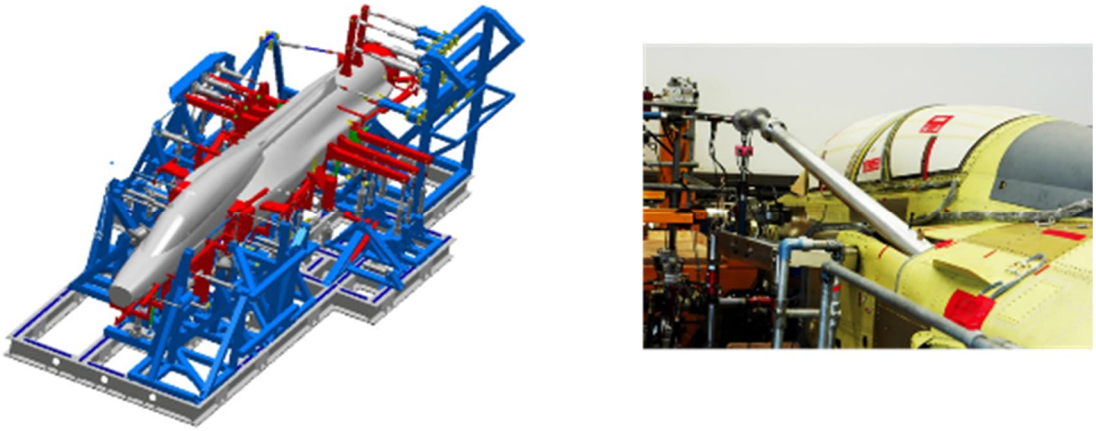

Figure 4.1-2. Full-scale fatigue test of Gripen D version, including the test of the refueling probe (left).

With the development of Gripen NG versions E/F, structural changes were made that related to several of the criteria for the need of test verification. Certification for airworthiness by full-scale testing is required due to:

- New mid fuselage/wing design, fuselage joints, MLG attachments
- Change of classification of parts due to design-for-manufacturing purposes
- Use of a new materials
- Increased basic design mass (~40% compared to C/D versions)
- New operational profiles

These structural changes call for a more extensive test programme than what was needed for the C/D versions. A full-scale static test (including impact damaged composite parts) of the complete airframe has been performed, see [1], and two full-scale fatigue tests of the complete airframes of E and F versions are currently planned to be tested in the same rig for 4 lifetimes, see Fig. 4.1-3. In addition to the full-scale fatigue test, control surfaces (not included in the test airframe) were tested in separate assemblies. These tests were combined fatigue and damage tolerance tests, initially cycled for 2 lifetimes without artificial initial defect followed by 2 lifetimes with artificially manufactured defects installed.

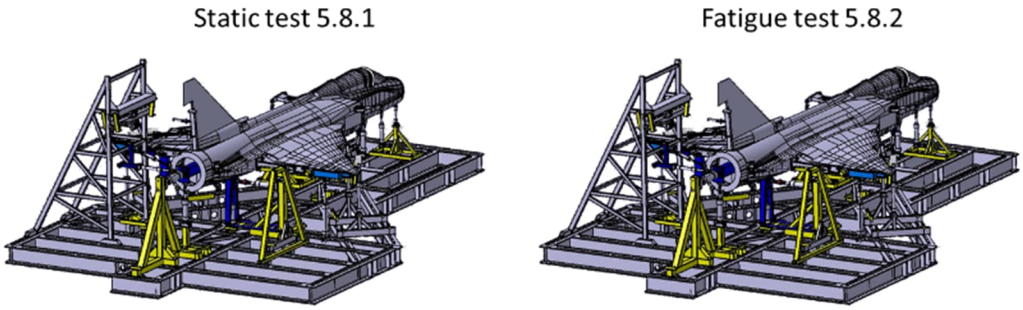

Figure 4.1-3. Full-scale fatigue tests of Gripen E version.

Full-scale tests of assemblies for compliance with damage tolerance requirements are also needed due to the structural changes in load paths and the upgraded classification of fuselage stringer joints and the design change of the wing to fuselage joint. To assure necessary and sufficient confidence regarding damage tolerance, a significant test effort designed to challenge typical airframe crack scenarios with part through cracks (surface cracks in thickness steps,

open and loaded holes etc.) was accomplished. Figure 4.1-4 shows structural objects/assemblies which are verified for damage tolerance when having multiple artificial initial defects installed in critical sections. Descriptions of most of these tests can be found in [1]-[4] and the elevon and the canard tests are presented in chapters 4.2 and 4.3 of this document. The full-scale fatigue test of Gripen F airframe is described in more detail in the following section.

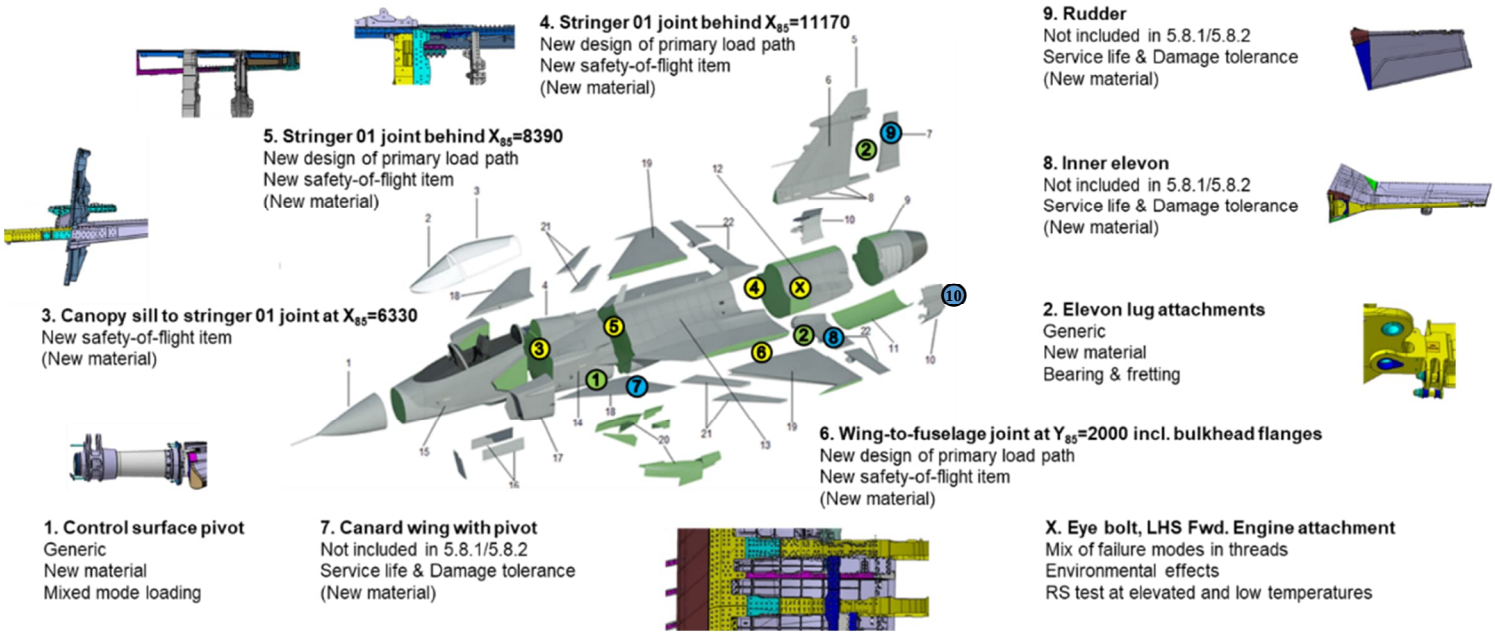

Figure 4.1-4. Full-scale damage tolerance tests of assemblies having artificial defects installed.

Full-scale fatigue test of Gripen F airframe

The primary objectives of this testing program are:

- **Validate Structural Service Life:** Confirm the structural integrity of the aircraft design by subjecting it to simulated service loads over an accelerated timeframe, equivalent to its full operational life.
- **Validate global Finite Element Analysis (FEA) Model:** Verify the accuracy and predictive capabilities of the global FE model by comparing test results with simulated load and deformation data.
- **Identify Fatigue-Critical Areas:** Detect any previously unknown areas susceptible to fatigue damage, allowing for targeted design improvements and maintenance strategies.
- **Establish Inspection and Maintenance Guidelines:** Utilize test data to establish evidence-based inspection intervals and potential structural modifications based on the observed extent of fatigue damage.

Test Rig Configuration

The dedicated test rig is engineered to apply precise and controlled loads to the test specimen, replicating real-world flight conditions. Key components include:

- **Robust Steel Frame:** A high-strength steel frame designed to withstand the demanding loads applied during testing.
- **Advanced Data Acquisition System:** An extensive network of approximately 800 strain gauges provides real-time data on strain distribution throughout the structure.

- **Hydraulic Actuation System:** 126 hydraulic cylinders enable precise control and application of various load profiles.
- **Pressurization System:** Eight pressure channels facilitate the pressurization of fuel tanks, cockpit, and air ducts, simulating in-flight conditions.

Test Specimen Configuration

The test specimen, designated 084, comprises a representative section of the aircraft structure:

- **Fuselage:**
  - Excludes radome and landing gear doors.
  - Includes pressurized fuel tanks, cockpit, and air duct.
- **Wings (Left and Right):**
  - Excludes control surfaces.
  - Includes pressurized fuel tanks.
- **Vertical Stabilizer (Fin):**
  - Excludes control surfaces.
- **General Exclusions:**
  - Non-load-carrying hatches are generally excluded, with some exceptions.
  - Pylons, control surfaces, landing gear, air intake, engine, tail cone, and aerial refueling probe are replaced with dummies.

This testing program will provide valuable insights into the fatigue behavior of the aircraft structure, contributing to the development of safer, more reliable, and durable aircraft designs.

Figure 4.1-5. Full-scale fatigue test set-up, Gripen F airframe.

References

[1] Z. Kapidžić. A review of aeronautical fatigue investigations in Sweden during the period April 2021 to March 2023. Presented at the 38th Conference of the International Committee on Aeronautical Fatigue and Structural Integrity, 2023.

[2] Z. Kapidžić. A review of aeronautical fatigue investigations in Sweden during the period April 2019 to March 2021. Presented at the 37th Conference of the International Committee on Aeronautical Fatigue and Structural Integrity, 2021.

[3] Z. Kapidžić. A review of aeronautical fatigue investigations in Sweden during the period April 2017 to March 2019. Presented at the 36th Conference of the International Committee on Aeronautical Fatigue and Structural Integrity, Krakow, Poland, 2019.

[4] JE. Lindbäck, Z. Kapidžić, A. Gustavsson, R. Laakso. Fatigue and damage tolerance testing of Gripen E/F rudder. 31st ICAF Symposium, Delft, 26-29 June 2023.

4.2 Fatigue and damage tolerance testing of Gripen E/F elevon

A. Gustavsson[1]

[1]Saab Aeronautics, Linköping, Sweden

Introduction

A structural test of Gripen 39E/F inner elevons was performed to verify the safe-life and damage tolerance of the elevon structure, see Fig. 4.2-1. Two different design load sequences, one representing the operational profile of 39E-version and the other for the 39F-version, with the latter being more severe, have been considered. The test was successfully run to a number of simulated flight hours where the most critical crack had grown from an artificial defect to a predicted critical length. A subsequent static test showed that the structure had sufficient residual strength.

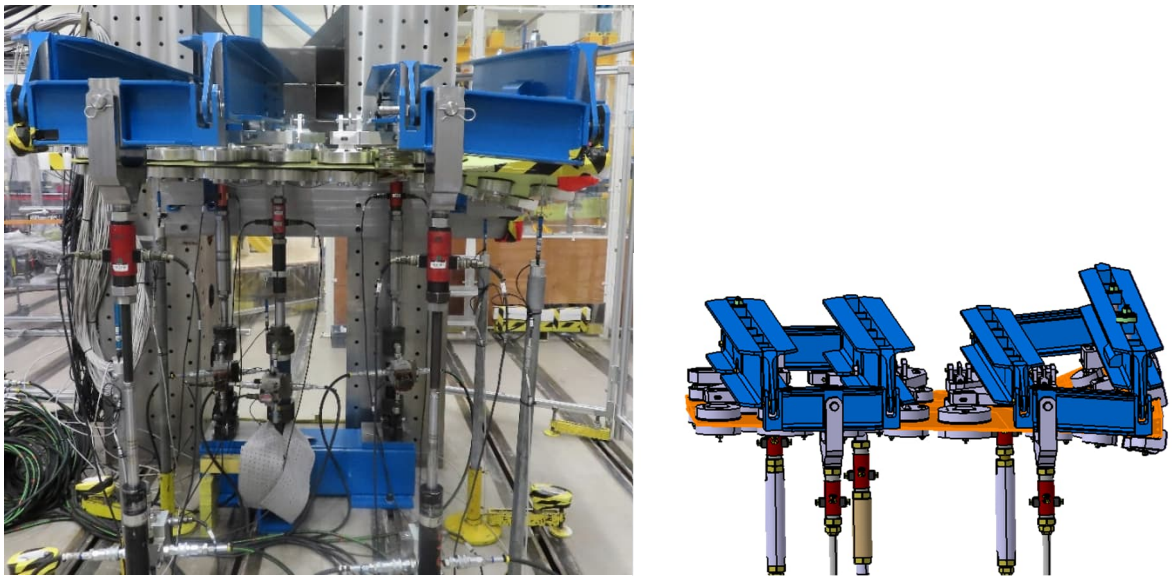

Figure 4.2-1. Inner Elevon Fatigue and DT-test object and test rig.

Loads

The loads on the inner elevons are based on air loads from complete aircraft, these are then applied with a link system. The loads are applied by five hydraulic actuators. Four of them (C1, C3, C5 and C6) are each connected to linkage and pad system that introduce loads on the elevon on both sides of the structure. The fifth actuator (C4) is load controlled on the middle bearing hinge. The test is performed in room temperature and dry condition.

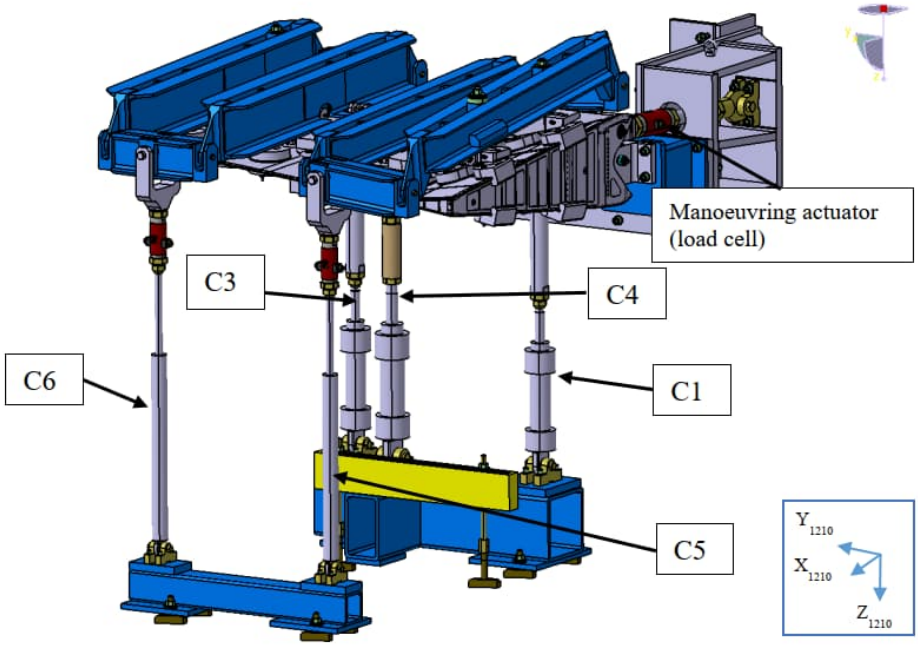

Figure 4.2-2. Inner Elevon Fatigue and DT-test configuration of load arrangement.

Test procedure

The focus was on the forward structure with the wing attachments. 6 artificial crack was introduced for the two last design lives. One crack in the bolt and the rest in the most critical points on the structure in lugs and radius.
The test structure was equipped with serval strain gauges with the purpose of monitoring the crack growth and to verify the DFEM models and crack growth analysis.
The test was run for 5.0 design lives in total. Although several cracks grew during the test, no failure or unstable crack growth occurred during the test sequence. A subsequent static test showed that the structure had sufficient residual strength.

Conclusion

The elevon tests were successful and the structures showed out to be robust from a fatigue respective a damage tolerance point of view. Test and DFEM shows good correlation for the strain gauges and displacements gauges. Crack growth was slower in test compared to analysis for all initiated cracks.

4.3 Fatigue and damage tolerance testing of Gripen E/F canard

JE. Lindbäck[1]

[1]Saab Aeronautics, Linköping, Sweden

Introduction

A structural test of Gripen 39E/F Canard was performed to verify safe-life and damage tolerance of the Canard structure, see **Error! Reference source not found.** 4.3-1. The test was performed in 2023-2024 in Linköping. The test scope was:

- To validate 4 design life fatigue strength by sustaining an initial 2 design life and to sustain another 2 design life in the Damage Tolerance part of the test.
- To validate no or limited crack growth for the 2 design life load spectrum in the Damage Tolerance part of the test. Before the start of the Damage Tolerance test, artificial flaws to be cut on defined critical parts.
- To show residual strength for selected static load cases to 120%LL after 4 design life.
- To cover both 39E and 39F.

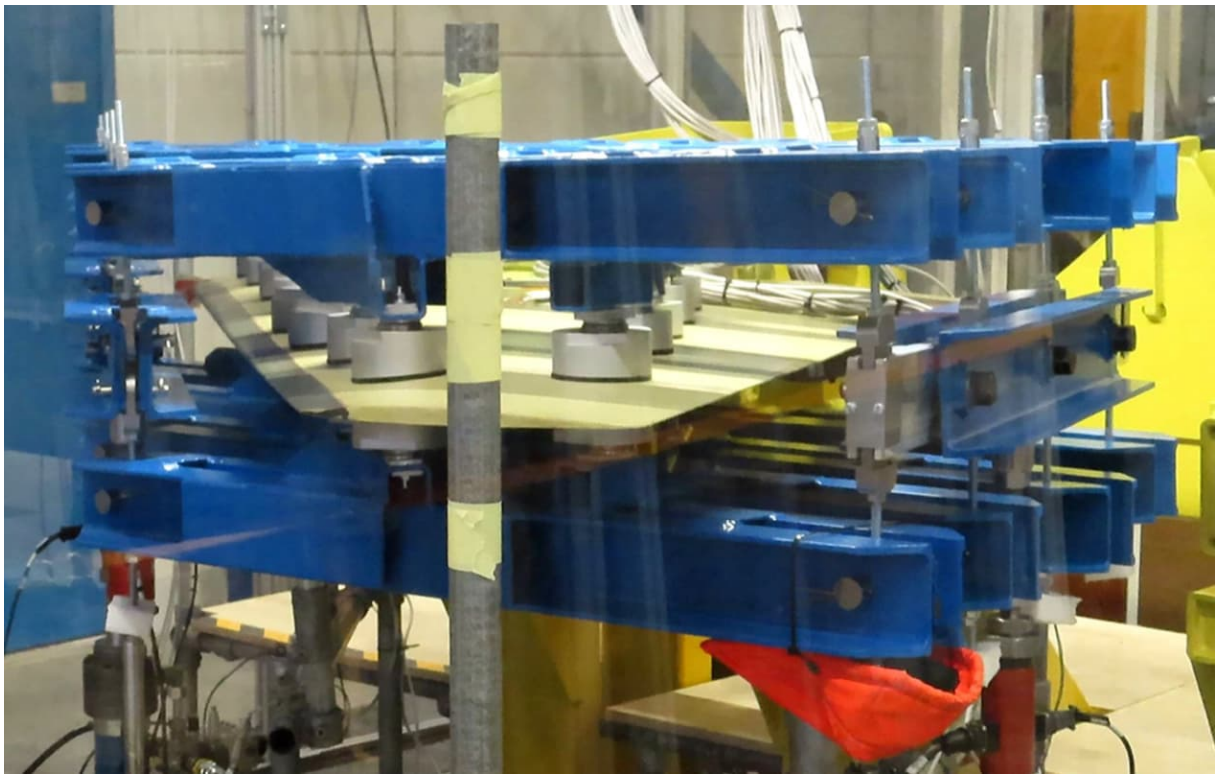

Figure 4.3-1. The Canard Wing in the test rig.

Loads

Three actuators applied the air loads via a whiffle tree to pads on both side of the Canard, see Fig. 4.3-1. Three critical static load cases were selected for the final residual strength test (RST). One of these static load cases, scaled to 80% limit load, was used as a reference load case applied several times during the test campaign to monitor any difference in gauge results. One finding was that a significant bearing friction was observed by comparing predicted jack

actuator load with loads from the load cell. The friction was initially as high as 17% but only about 7% at the end of the test campaign. The effect of friction is further discussed below.
A 39E load sequence was run with 8000 flh.

Test procedure

The two first design lives were run without artificial defects and the following two lives with artificial defects at the aluminum pivot and moment arm.
Due to the crack growth rate and crack length found, RST was first performed after

- 28 000 Flh: In order not to have a failure when performing RST
- 32 000 Flh: In order to verify full life for 39E
- 32 800 Flh: In order to verify extra hours for 39F (Crack size had reached theoretical critical size)

The effects of crack closure after RST at 120%LL was handled by removing the time from RST to when the two major cracks started growing again from the total accumulated time. This could be done as the strain gauges showed the effects of crack growth very well for these cracks. The cracks started to growth directly after restart of the test and there was no need to correct any time for the DT test.

After 32 800 Flh the RST was performed successfully. The most critical load case was increased until failure which happened at 166% LL. The RST load cases was upscaled due to the observed friction. For the fatigue loads was friction already considered in the load spectrum.

Conclusion

The crack growth rate for the most critical cracks were monitored thoroughly during the latest phase of the test campaign and after failure was the cracks opened and studied in microscope. The most critical crack 2.3.1c is further described below, see Fig. 4.3-2. Failure occurred for crack 2.3.1c at the pivot axes, see micrograph in Fig. 4.3-3.

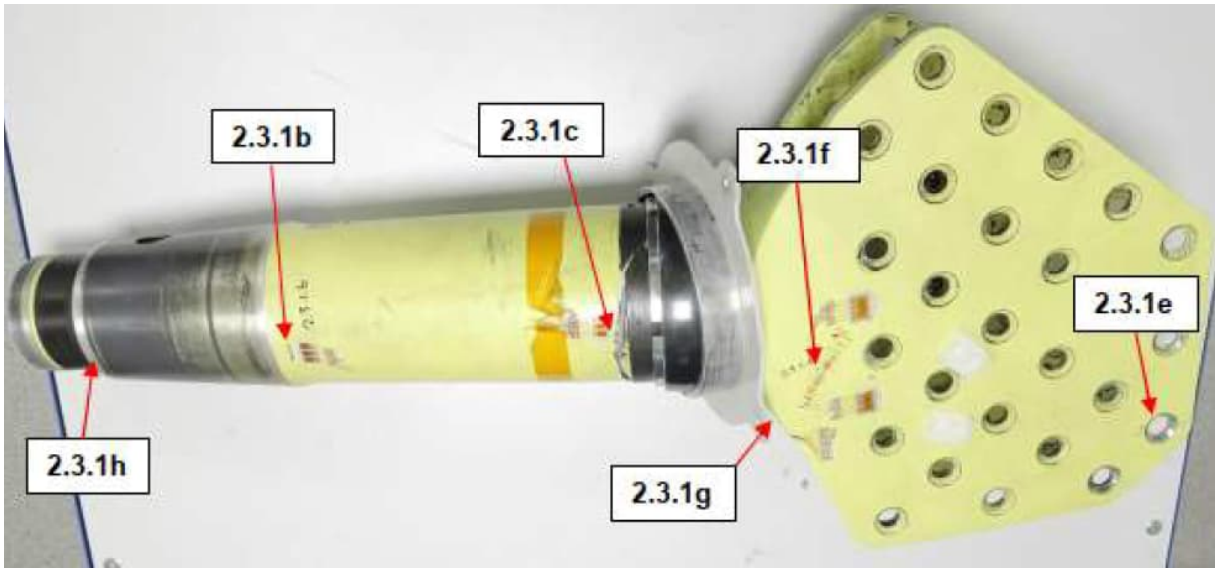

Figure 4.3-2. Positions of cracks that have shown growth during the test.

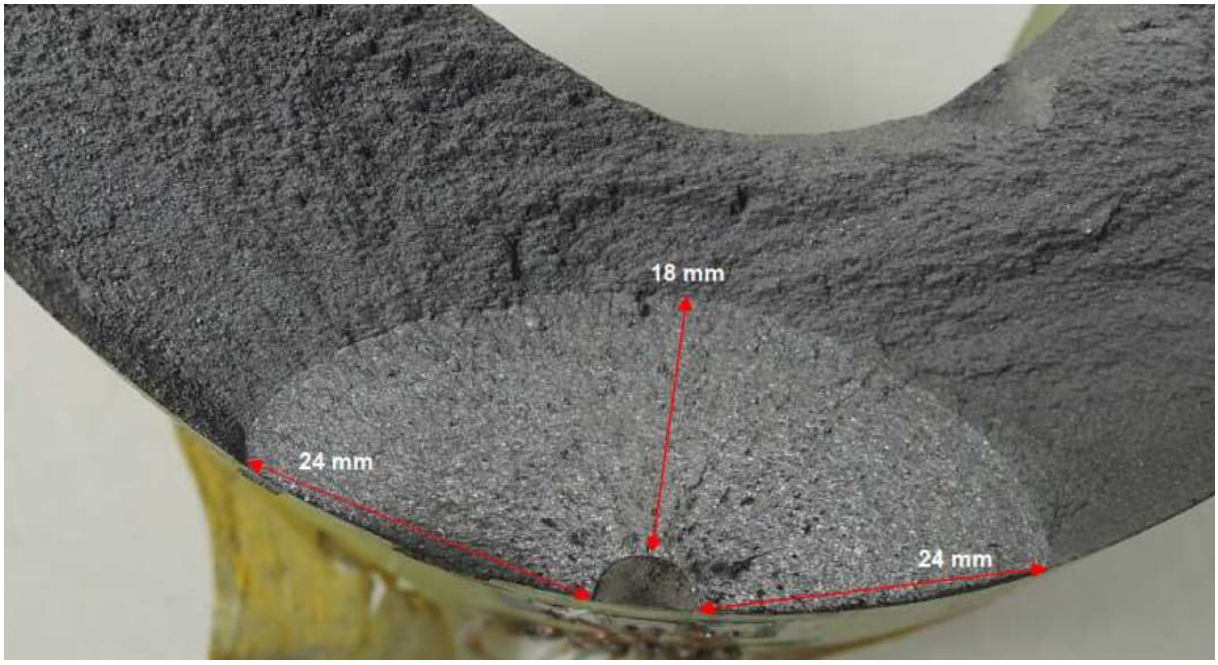

Figure 4.3-3. The fatigue crack surface in position 2.3.1c. Red arrows indicate the fatigue crack.

The artificial crack (a=c=3.175mm) is the small grey area at the bottom and the fatigue crack is the lighter area, also measured in the figure.

By using the Wheeler crack retardation model with a value of 0.4 in AFGROW, the following curve is obtained which will give failure at 16800 flh (32800 - 2*8000 = 16800) but with a higher critical crack length compared to the test. This is still deemed conservative which can be shown by increasing the Pxx value in AFGROW to 166% LL (which is where the test broke) and noting that a smaller critical crack length is observed in the analytical solution compared to the test, see Fig. 4.3-4.

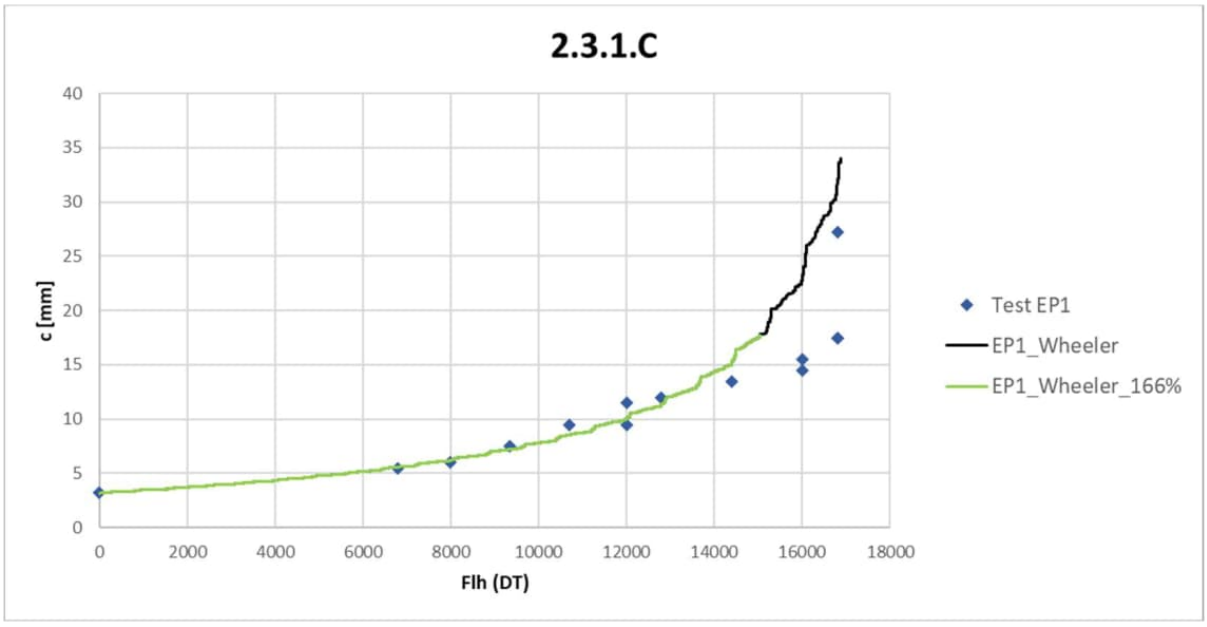

Figure 4.3-4. Crack length vs flight hours for analytical crack growth without user defined Kmax and with Wheeler-factor 0.4 compared to test results.

The Canard was validated for Fatigue and DT for a full 39E life. The calculation methodology for the Canard is validated by the test for 39E. As the same calculation methodology was used

to analytically obtain full fatigue life from a durability point of view for 39F, full fatigue life with respect to durability could be considered to have been verified by the test also for 39F. For DT the test has verified 75% of the 39F life.

5 ADVANCED MATERIALS AND INNOVATIVE STRUCTURAL CONCEPTS

5.1 Static and fatigue testing of specimens made with linear Friction Stir Welding (FSW)

Z. Kapidzic[1], *S. Borgenwall*[1], *V. Patel*[2]

[1]Saab Aeronautics, Linköping, Sweden
[2]University West, Trollhättan, Sweden

Introduction

Friction Stir Welding (FSW) is a solid-state, sustainable joining process that uses frictional heat and mechanical pressure to weld materials without melting them. Compared to conventional fusion welding, FSW reduces the energy consumption, emissions and waste, as it does not require filler materials. Also, FSW induces less alloy element volatility and defects than traditional fusion welding. In particular, FSW is suitable for joining of thin-walled aluminum components because it and enables welding of different alloy types, for instance 2xxx and 7xxx series aluminum, and is therefore a viable replacement for riveted and bolted joints. There are several potential benefits that can be gained using FSW compared to riveting. For instance, the FSW processing zone involves recrystallization, grain refinement and homogenization of hardening particles which typically improves the mechanical material properties of aluminum. Another advantage, compared to bolted joints, is that FSW eliminates the need for hole drilling and fastener installation.

Within the collaborative research project InteDemo [1], Saab and University West conducted studies focusing on evaluating the feasibility and mechanical performance of FSW aluminum joints. Several multi-plate panels were manufactured using FSW, of which one was used as a part of a rear fuselage demonstrator. Figure 5.1-1 shows one of the manufactured panels.

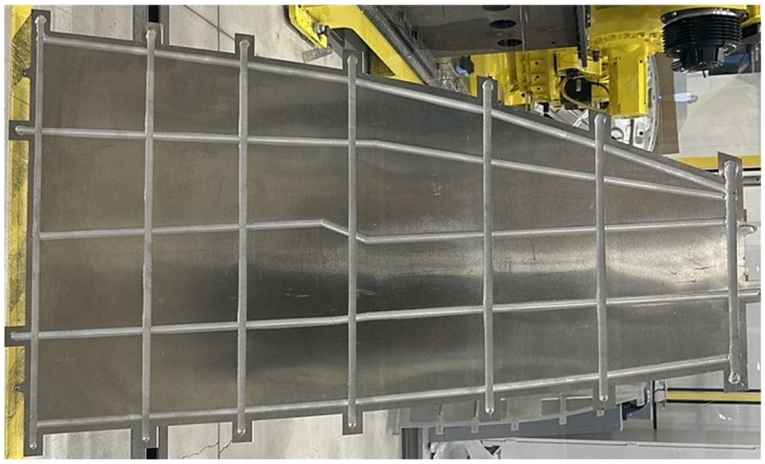

Figure 5.1-1. One of the FSW panels manufactured in the IntDemo project.

In the experimental part of the study, the static and the fatigue properties, as well as the failure behavior of continuous linear FSW joints was evaluated by conducting mechanical tests on coupon specimens. The aim was to assess the potential of linear FSW joints in comparison to

well-stablished properties of bolted/riveted joints with similar joint geometry. The test procedure and results are briefly presented below.

Coupon testing procedure

Coupon specimens were cut out from three FSW welded panels, constituting single-shear butt lap joints with two skin plates and a lap plate. The plates were joined with four linear welds made with a 5 mm diameter weld pin, as shown in Fig. 5.1-2Figure. Two types of specimens were manufactured:

- Type A1, with skin plates made of AA2024-T3 and joint plate made of AA7475-T761
- Type A2, with skin plates made of AA7475-T761 and joint plate made of AA7475-T761.

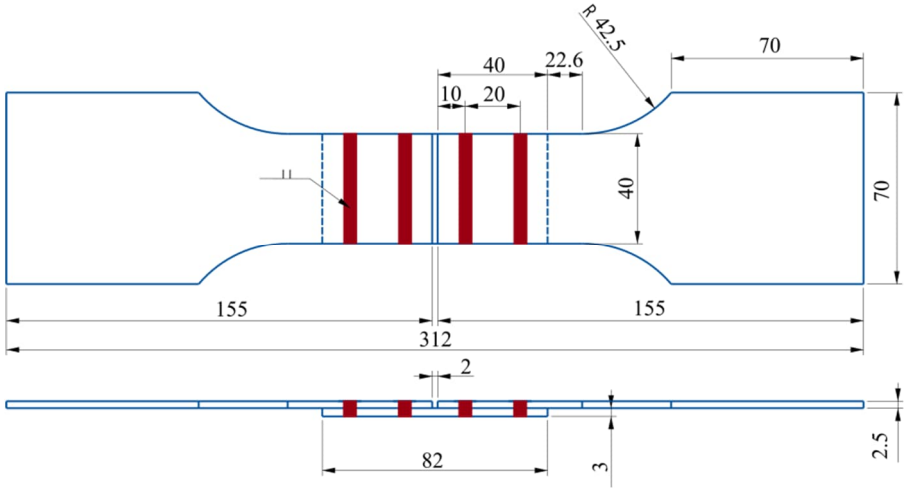

Figure 5.1-2. Test coupon geometry and dimensions in mm.

All tests were performed in a tensile machine using a two-piece lateral support to reduce the secondary bending, similar to the one described in [2]. Three types of loading procedures were conducted:

- **Static loading** to failure, performed on 2 specimens of each type.
- **Constant amplitude** (CA) **loading** at R = 0, performed on 10 specimens of each type.
- **Spectrum loading** to failure, performed on 6 specimens of each type. The sequence consisted of 57 cycles/flh and was created by removing all negative states from a typical fighter wing bending moment sequence, see the spectrum plot for 1000 flh in Fig 5.1-3. The reason for removing the negative states was to not risk specimen buckling.

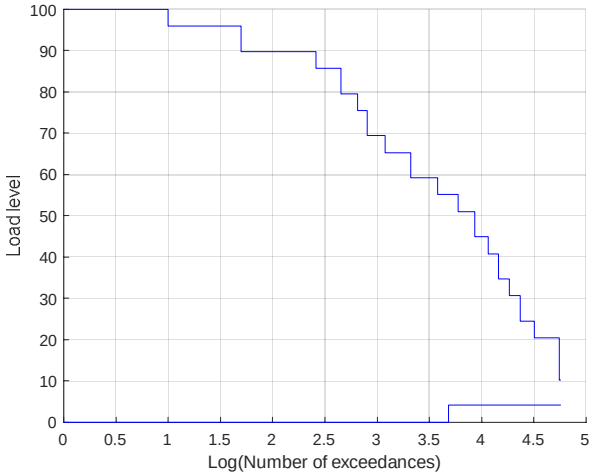

Figure 5.1-3. Exceedance plot for the test sequence, 1000 flh.

Results

Figure 5.1-4 shows the a applied gross skin stress-displacement curves, together with the yield stress, Rp02, and the tensile strength, Rm, for the skin plate materials. The specimens of type A1 (AA2024-T3/AA7475-T761, blue curves) start to yield at approximately the level of Rp02 for AA2024-T3 and fail at somewhat lower stress than Rm for AA2024-T3. There is a significant amount of plastic yielding before failure. On the other hand, specimens of type A2 (AA7475-T761/AA7475-T761, red curves) fail in a brittle manner at a significantly lower stress than Rp02 for AA7475-T761. Both specimen types (A1 and A2) failed at one of the outermost welds, as shown in Fig. 5.1-5.

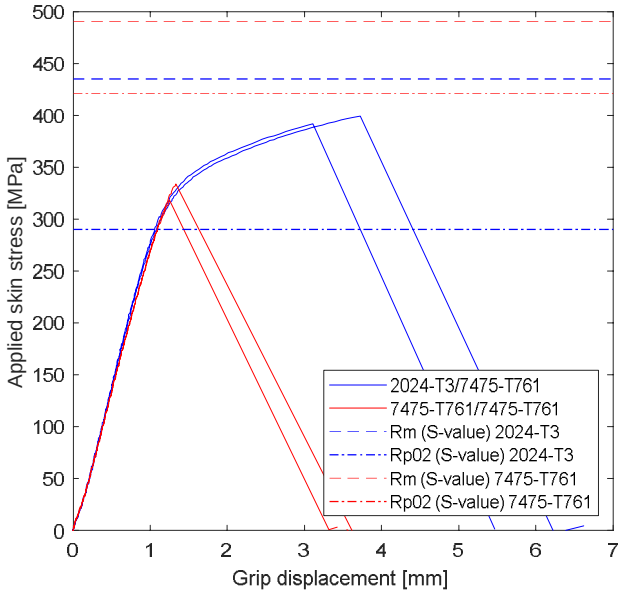

Figure 5.1-4. Applied gross skin stress-displacement curves.

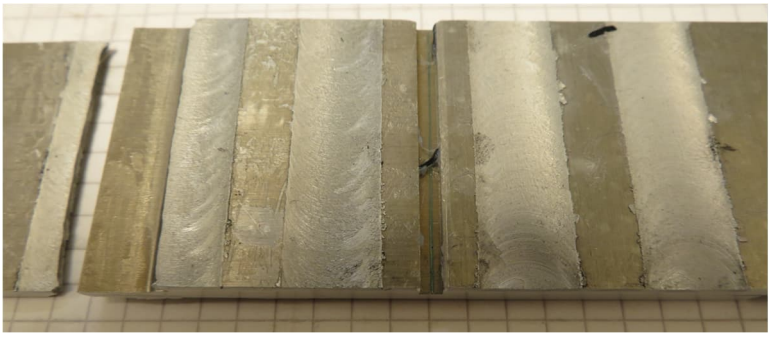

Figure 5.1-5. Static failure.

Using a method from [3], predictions of CA fatigue life were made assuming that the FSW specimens will have similar fatigue life as bolted (denoted BJR 3526) or riveted (denoted RJR 3526) specimens made of 2024 material. The predictions are shown together with the test results in Fig 5.1-6. The comparison showed that specimens A1 (AA2024-T3/AA7475-T761) have similar fatigue life as predicted, while specimens A2 (AA7475-T761/AA7475-T761) have about 20-30% lower fatigue strength.

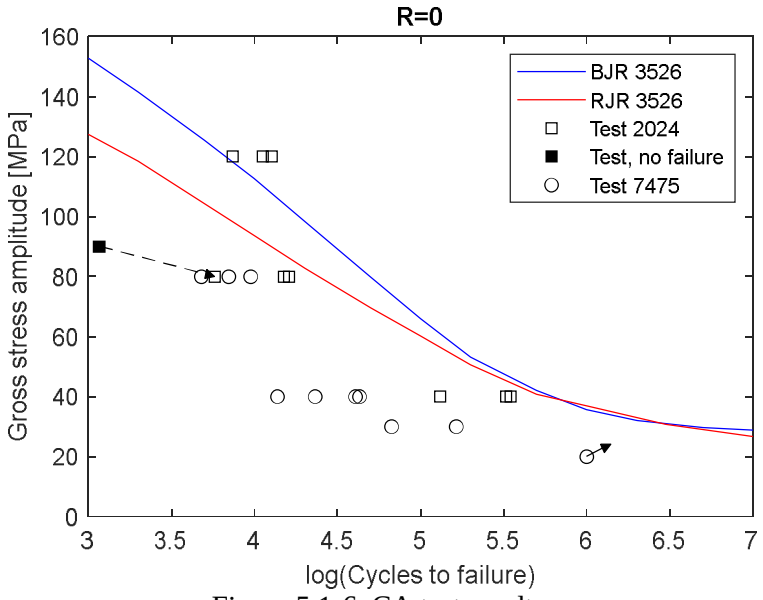

Figure 5.1-6. CA test results.

Both specimen types failed at one of the outermost welds, similarly to the static specimens. The fatigue cracks typically initiated in the skin plate at the faying surface and subsequently coalesced into a large crack that grew almost all the way through the thickness. The fatigue cracks in type A1 specimens were mostly planar, see Fig. 5.1-7 while the cracks in type A2 specimens had a rough surface with multiple crack initiation points.

Figure 5.1-8 shows the results from the spectrum tests together with the predictions for bolted and riveted joints. The same trend is observed as in CA tests, namely that specimens A1 (AA2024-T3/AA7475-T761) have similar fatigue life as predicted while specimens A2 (AA7475-T761/AA7475-T761) have shorter fatigue life. The observed failure modes were also similar to those observed in CA tests.

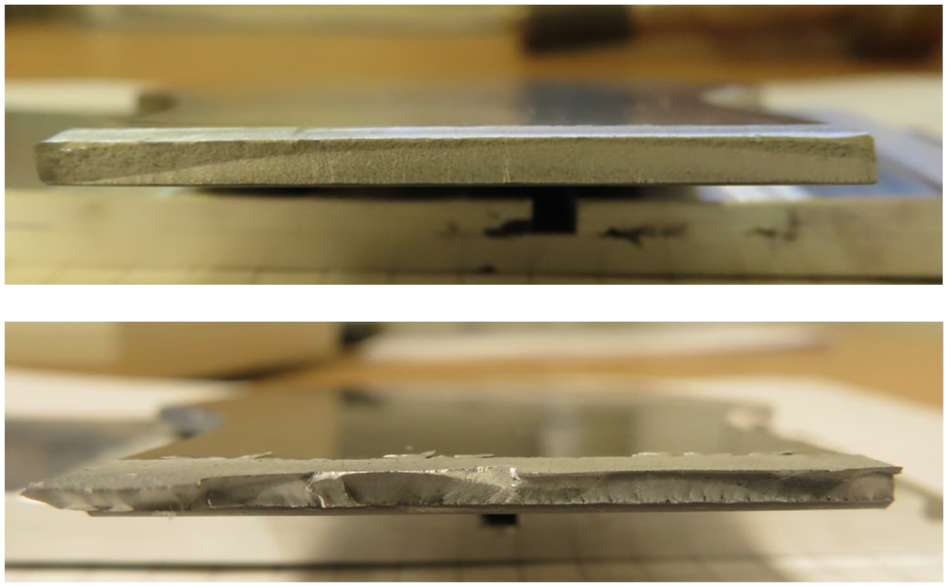

Figure 5.1-7. Specimen A1 (upper) and A2 (lower) skin plate cross section after failure. Faying surface downwards.

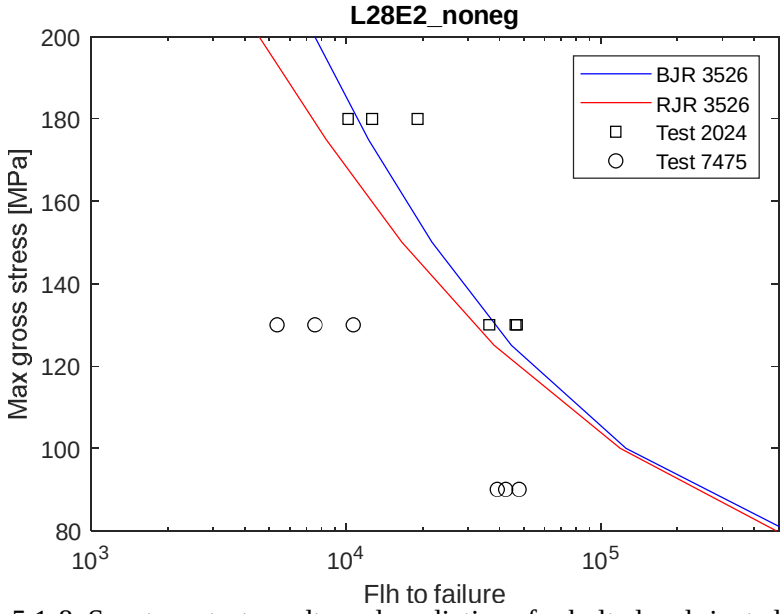

Figure 5.1-8. Spectrum test results and predictions for bolted and riveted joints.

Conclusions

Static and fatigue tests of linear FSW joint specimens made with two aluminum material combinations, AA2024-T3/AA7475-T761 and AA7475-T761/AA7475-T761 were performed. The tests showed that the static and fatigue strength of the combination AA2024-T3/AA7475-T761 was 20-30% higher and approximately equal to the strength of similar bolted/riveted joints.

References

[1] https://www.hv.se/en/research/research-projects/production-technology/multifunktionell-skrov-demonstrator/

[2] Z. Kapidžić, D. L. Ávila Granados, J. A. Moreno Arias, M. J. Quiroga Aguilera, J. P. Casas Rodríguez, J. C. García Callejas. Bolt fatigue in CFRP joints, International Journal of Fatigue, 164, 107138, 2022.

[3] TKH-R-3373. Utmattningshållfasthet hos skruvförband i aluminium vid bestämning med en geometriskt baserad omräkningsmetod. (Saab internal document in Swedish).

6 FATIGUE LIFE ENHANCEMENT METHODS AND REPAIR SOLUTIONS

6.1 Testing of repairment method EPOCAST for incorrectly drilled bolt holes in CFRP joints

Z. Kapidzic[1]

[1]Saab Aeronautics, Linköping, Sweden

Carbon fiber reinforced polymer (CFRP) plates are commonly joined using bolted connections. In large airframe panels the connections can have a large number of bolts which are installed after co-drilling the plates. During the drilling operation, there is a risk that the bolt holes can be incorrectly drilled. For example, a hole can be mislocated, drilled with an angularity outside of tolerance or too deeply countersunk. In such cases a repairment might be an option. However, the effect of the repairment on the strength of the joint need to be accounted for.

In this study, a two-step repairment technique using Epocast potting is investigated. The study is currently ongoing as a collaboration between Saab AB in Sweden and CIAC and University of Los Andes in Colombia. Epocast 1635 consists of a two-component epoxy resin that is mixed with aluminum powder. It can be applied using a mixing nozzle to ensure a good mixture of components. The repair is performed in two steps by first repairing the incorrectly drilled hole and then drilling a correct hole, partially through the repair. Figure 6.1-1 shows an example of the repairing procedure and a repaired countersunk hole.

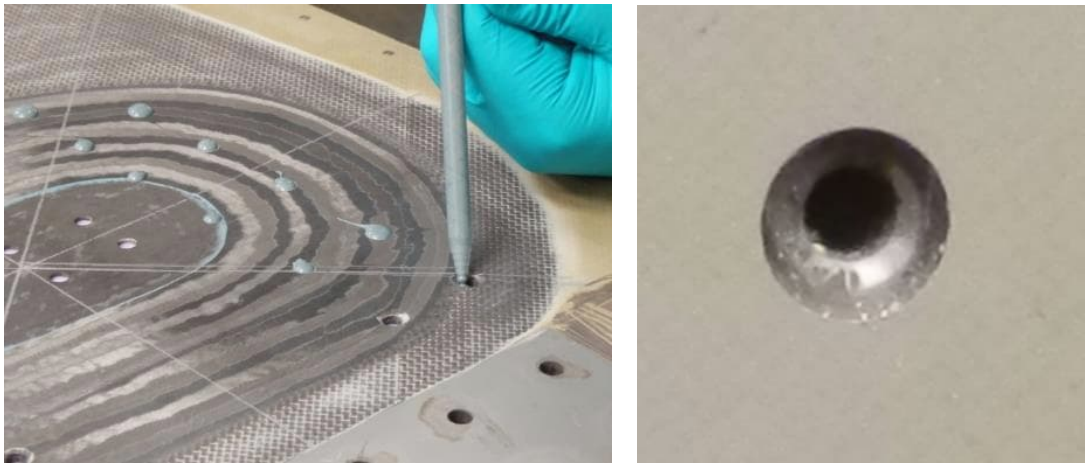

Figure 6.1-1. Repairing of incorrectly drilled holes using Epocast potting.

The study aims at establishing knock-down factors for bearing strength, net-section strength and fatigue strength of repaired holes. Three different types of incorrect drilling are considered, as shown in Fig. 6.1-2, misplaced holes and too deeply countersunk holes. The experiments are being performed on standard specimens and include variations of laminate layup, thickness, hole diameters, static, constant amplitude and spectrum loading. Some of the specimens have been cut through the repaired hole and the cut sections were investigated by fractography. Figure 6.1-3 shows the fractography images of three different hole reparation types. So far, the resulting repairs look promising.

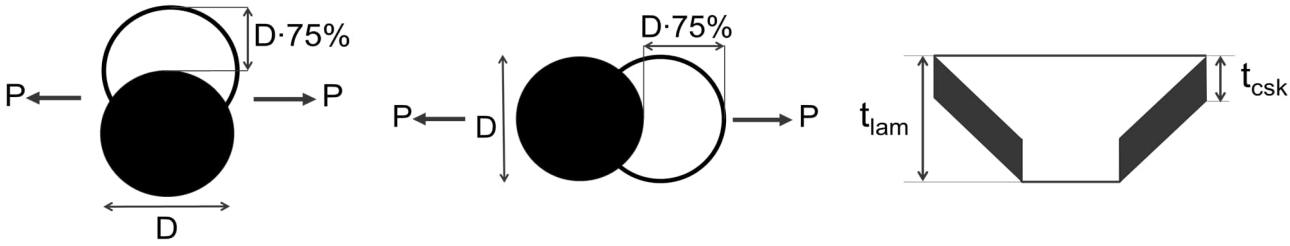

Figure 6.1-2. Types of incorrectly drilled holes.

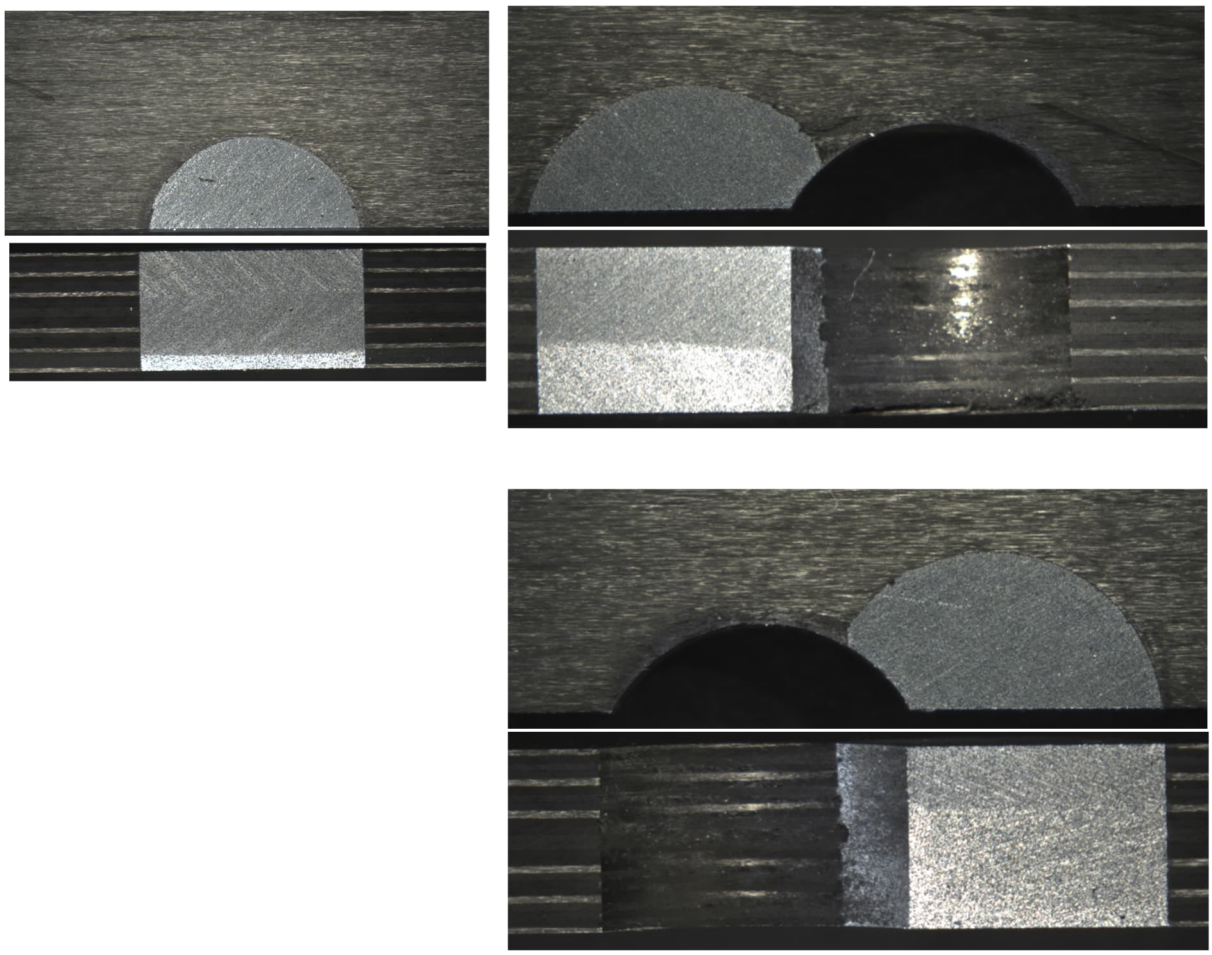

Figure 6.1-3. Top and cross-section views of the cut-up specimens.

6.2 Surface postprocessing to improve fatigue strength of AM titanium

M. Kahlin[1]

[1]Saab Aeronautics, Linköping, Sweden

Background

Previous studies of additively manufactured Ti6Al4V have shown that the fatigue properties are dominated by the rough surface rather than internal defects [1]. Consequently, the surface roughness should be improved before additively manufactured parts could be introduced to more critical structural aerospace applications. Fatigue testing has shown that L-PBF Ti6Al4V subjected to hot isostatic pressing (HIP) followed by traditional machining can achieve fatigue properties similar to conventional wrought Ti6Al4V [1]. However, to be able to use the potential of AM for structural aerospace parts, it is important that the inherent ability to manufacture complex geometries with AM can be used to increase part performance or reduce weight. In this study the effect of the chemical-electrochemical surface treatment Hirtisation was evaluated. Test specimens were produced in Ti6Al4V material with 60 µm build layer using an EOS M290. The specimens were printed to final dimensions (total length 80 mm and diameter 6.5 mm) resulting in a rough as-built surface in the gauge section, see figure above. One test series was further subjected to Hirtisation and the results were compared to as-built specimens and specimen with machined surfaces (machined from cylinders to the same final geometry).

Results

Hirtisation improved the fatigue strength considerably compared to specimens remaining in the as-built condition. The hirtisation specimens had fatigue strength in the same range as specimens with machined surfaces as illustrated in figure below.

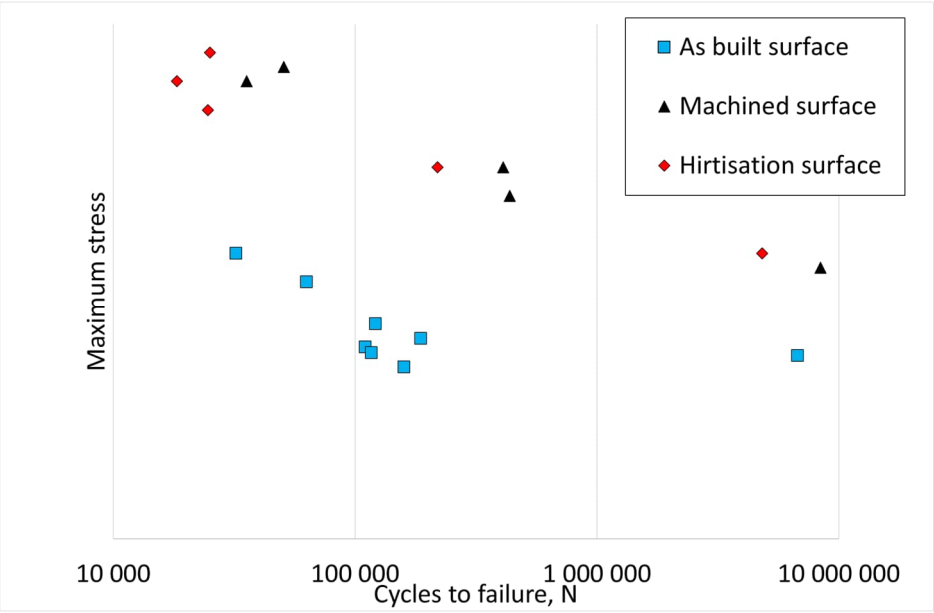

Figure 6.2-1. Fatigue results for AM Ti6Al4V with different surfaces.

References

[1] Kahlin M, Ansell H, Moverare JJ. Fatigue behaviour of notched additive manufactured Ti6Al4V with as-built surfaces. Int J Fatigue 2017, https://doi.org/10.1016/j.ijfatigue.2017.04.009.

6.3 Testing of cold spray for repair of aircraft components

T. Lindström[1]

[1]Saab Aeronautics, Linköping, Sweden

Cold spray is a manufacturing technology that, similar to other additive manufacturing techniques, builds up material in a layer-by-layer fashion. In contrast to other additive manufacturing techniques, cold spray operates at temperatures below the melting temperature of the material, which makes it favorable for repair since the part becomes less sensitive to distortion, residual stresses and microstructural changes. Cold spray has traditionally been used to create coatings, but due to the low operating temperature, the process has raised interest and can be used for repair of several types of damage.

In order to decrease cost and environmental impact, there is always an interest from the aerospace industry to minimize replacement of parts. Hence, cold spray could potentially be used to extend the life of parts where, instead of replacement, the damage is removed through machining, and the part is later restored to final dimensions using the cold spray technology.
In the proposed study, which will be performed at Saab AB in Sweden, the structural ability of cold spray as a repair process for aluminum alloys, commonly used in aircraft applications, will be investigated. The aim is to study if repairing damages with cold spray can increase the life of components compared to unrepaired material. Standard test geometries for tensile and fatigue testing will be investigated, where unrepaired material will be represented by grooves or notches in the standard test geometry. The groove or notch is then filled with cold spray, machined to final dimensions, and compared to unrepaired and undamaged material. For an example of such tensile and fatigue specimen, see Fig. 6.3-1. The unrepaired samples then act as a baseline, and a comparative measure of the fatigue and tensile performance of the repair can be established. A similar investigation has also previously been performed in [1].

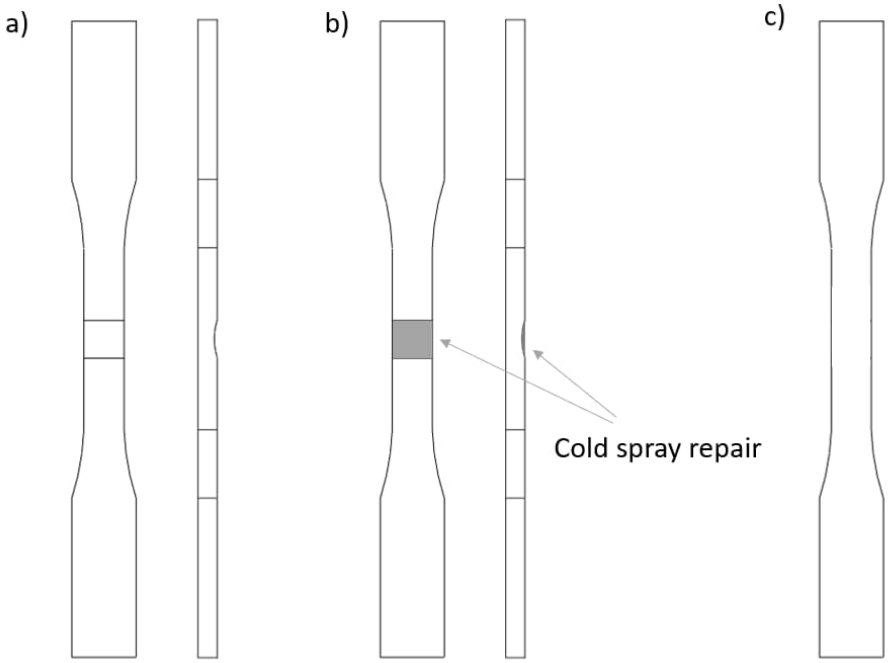

Figure 6.3-1. Example of test specimen representing a) damaged material with a groove/notch, b) repaired material, and c) undamaged material.

Additionally, to study the strength of a cold spray repaired hole, bearing strength tests will be performed on specimens with cold spray material around the hole. Such testing would also be representable for repairing incorrectly drilled holes for joints. In Fig. 6.3-2, three different types of cold spray repairs for the planned bearing strength testing are illustrated.

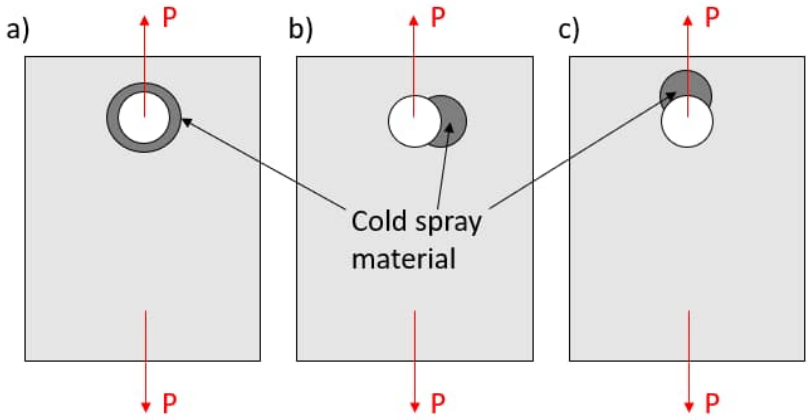

Figure 6.3-2. Three types of cold spray repairs around holes that will be tested.

References

[1] S. E. Galyon Dorman, J. W. Rausch, M. J. Ausherman and G. A. Shoales, Evaluation of Cold Spray for Aircraft Repair, 31st ICAF Symposium, 2023.

7 NDI INSPECTIONS AND STRUCTURAL LOAD/HEALTH MONITORING

7.1 NDT of additively manufactured titanium

M. Kahlin[1]

[1]Saab Aeronautics, Linköping, Sweden

Background

Non-destructive testing of additively manufactured metals is challenging due to, for example, rough as-built surface, small internal defects and lack of acceptance criteria in standards. In this project we focused on the challenges with the rough as-built surface from laser powder bed fusion process and detection of the defect type lack-of-fusion (LoF) using computed tomography (CT) and 2D X-ray (RT). Artificially manufactured defects (CAD seeded defects) were introduced into the test specimens in order to simulate LoF defects. This approach offers a method to control size and position of the defects aiming ultimately at procedures for resource efficient and safe POD derivation procedures. Test specimens were produced in Ti6Al4V material with 60 µm build layer using an EOS M290 with CAD seeded defects in the range of 100 µm to 400 µm. Specimens with both as-built and machined surface were evaluated.

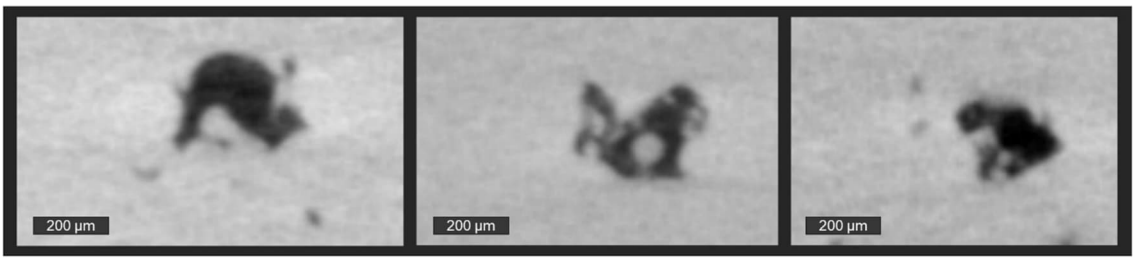

Figure 7.1-1. CAD seeded defect 2D XCT slices with similar appearance as LoF.

Results

The CAD seeded defects, especially with the small sizes, look very similar to real process induced LoFs both compared in light microscopy and the RT images, see Fig. 7.1-1. RT inspection detected all defects with size 200 µm and above regardless if the surface was as-built or machined. For smaller defect sizes the detection rate was higher for specimens with machined surface as illustrated in Fig 7.1-2.

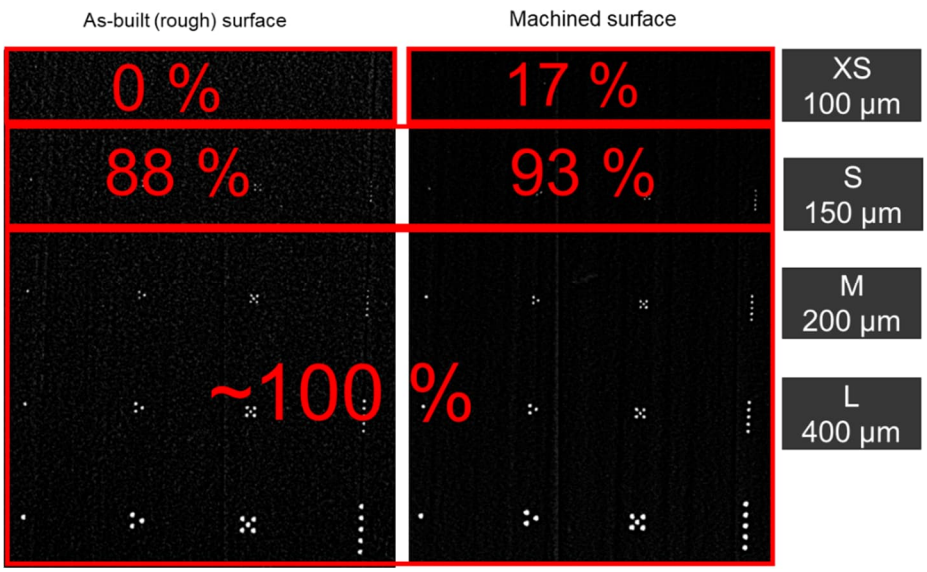

Figure 7.1-2. Detection rate for RT with pixel size 30-40 µm.

8 ACKNOWLEDGEMENTS

This editorial work was supported by Saab AB. The editor is also indebted to the following individuals who helped to write this review:

Hennes Wemming	Saab AB/LiU
Jan-Erik Lindbäck	Saab AB
Allan Gustavsson	Saab AB
Petter Haugskott	Saab AB
Stefan Borgenwall	Saab AB
Emma Lundqvist	Saab AB
Magnus Kahlin	Saab AB
Thomas Lindström	Saab AB
Stefan B. Lindström	MiUn
Mohamed Loukil	LiU
Vivek Patel	HW